

Rise and fall of vegetation primary production resilience to climate variability anticipated by a large ensemble of Earth System Models' simulations.

non-peer reviewed preprint submitted to EarthArXiv

Matteo Zampieri^{1*}, Bruna Grizzetti¹, Andrea Toreti¹, Pierluca De Palma² and Alessio Collalti³

¹European Commission - Joint Research Centre (JRC), Ispra IT

²Fincons SPA, Vimercate IT

³Institute for Agriculture and Forestry Systems in the Mediterranean, National Research Council of Italy (CNR-ISAFOM), Perugia (PG), Italy

*matteo.zampieri@ec.europa.eu

Abstract

Climate change is affecting many aspects of natural ecosystems and society. Anticipating the changes in vegetation resilience – the plants' capacity to cope with disturbances and shocks such as those related to climate variability and extremes – is critical to understand and project ecosystems' responses to global change and the impacts on the related ecosystem services, to support mitigation actions, and to define proper adaptation plans.

Here, we quantify vegetation gross primary production (GPP) resilience by computing the annual production resilience indicator from the state-of-the-art Earth System Model (ESM) simulations included in the newest Sixth Phase of the Coupled Model Intercomparison Project (CMIP6). Taking the present period (1985-2014) as reference, we estimate the GPP resilience changes for different periods in the near and far future (2021-2050 and 2051-2100) under three scenarios of socioeconomical global changes, corresponding to different levels of greenhouse gases' emissions and land-use.

In the 'Sustainability (Taking the Green Road)' and 'Middle of the Road' scenarios considered here (ssp126 and ssp245), the areas where vegetation shows increasing GPP resilience (mainly boreal, African and Indian monsoonal regions) are wider than the areas with decreasing resilience. The situation drastically reverses in the 'Fossil-fuel Development (Taking the Highway)' scenario (ssp585), mostly because the increase of GPP interannual variability outbalances the mean increase due to the CO₂ fertilization effect in this high greenhouse gases' emission scenario. Among the larger countries, Brazil is exposed to the highest risk of experiencing years with anomalously low GPP, especially in the 'Taking the Highway' scenario.

Introduction

Stable ecosystems, characterized by small variations from their average state despite changes in environmental conditions, are generally considered healthy and reliable in terms of the services they provide (Costanza et al., 2014; MAE, 2005; Seddon et al., 2019). Ecosystems in good condition are necessary to secure the sustainability of human activities and human well-being (Maes et al., 2020). There is currently great concern about the stability and resilience of both natural and human-managed ecosystems, particularly given the many global changes that are already occurring, such as land use and climate change (IPBES, 2018; Williams et al., 2014). The Sustainable Development Goals, formally embraced by the 2010 Conference of Parties, recognize the importance of ensuring conservation, restoration and sustainable use of terrestrial ecosystems and their services, and strengthening the resilience and adaptive capacity to climate-related hazards (SDG 15 and SDG 13, respectively; United Nations 2016).

The concept of resilience is closely connected to ecosystem stability. Resilience has been defined either as the larger disturbance that a system can absorb without losing its structure, relationships and functionalities (Holling, 1996, 1973) or as the time required by an ecosystem to recover and return back to the equilibrium state after a disturbance (Pimm, 1984). These definitions are termed 'ecological resilience' and 'engineering resilience', respectively. On the one hand, ecological resilience is a very powerful concept as it comprehensively accounts for the complexity of the ecosystem structure (e.g., total biomass, population distribution, diversity) and function (e.g., primary production, pollination) but is difficult to define quantitatively (Oliver et al., 2015). On the other hand, the engineering definition of resilience is more specific in suggesting a quantitative measurement method that was inherited by the classical theory of population dynamical systems such as the Lotka-Volterra model (Lotka, 1920; Volterra, 1926).

In the case the ecosystem analysis is focused to gross primary production (GPP), the two definitions of resilience can be in principle consistent between each other (Zampieri, 2021). GPP

— the total carbon fixation by plants — is a primarily important terrestrial ecosystem function, at the point that it was also considered as a proxy of resilience itself (Moore et al., 1993). This essential biological process provides the base of the net primary production determining the plant growth and the main input for the food chain of myriad animal consumers including humans (Richmond et al., 2007; Vargas et al., 2019). GPP also controls the rate at which carbon dioxide is removed from the atmosphere while being at the same extremely sensitive to climate anomalies itself (Ciais et al., 2005; Raupach et al., 2007; Seddon et al., 2016).

Assessing the changes of vegetation GPP resilience of vegetation GPP in the future climate scenarios is of capital importance. Climate change is indeed expected to alter vegetation GPP resilience by potentially compromising the availability of water for natural vegetation and agriculture in dry regions (Betts et al., 2018; Stuart-Haëntjens et al., 2018; Zampieri et al., 2019) and in general by increasing the frequency, amplitude and duration of extreme events that are detrimental for vegetation productivity (Dosio et al., 2018; Naumann et al., 2018; Pokhrel et al., 2021; Toreti et al., 2019). At the same time, the increase of atmospheric CO₂ concentration coming along with global warming is expected to bring positive effects in terms of vegetation photosynthetic rate i.e. the so called 'CO₂ fertilization effect' (Sage and Kubian, 2007) and water use efficiency (Peters et al., 2018), although uncertainties remain (e.g. on acclimation) and the positive effects are expected to level off at around 600ppm (Bastos et al., 2020; Toreti et al., 2020).

To better represent the interactions between climate and vegetation primary production, climate models recently evolved in a direction that includes a comprehensive dynamical representation of the carbon cycle, amongst other development lines (Randall et al., 2019). Since the early 1990s, General Circulation Models (GCMs) estimate the solution to three-dimensional differential equations of fluid motion and thermodynamics to obtain time and space dependent values for temperature, winds and currents, moisture and/or salinity and pressure in the atmosphere and ocean (Mitchell et al., 1995; Murphy, 1995; Sausen et al., 1988).

The importance of an accurate and interactive representation of land surface processes such as surface hydrology as well as the role of vegetation in modulating energy and water budgets and determining relevant surface variables such as temperature and soil moisture was soon recognized (Bonan, 1998; Dickinson et al., 1998). Although the spatial resolution of the GCMs grid could have been rather low, it is worth noting that these models accounted for the sub-grid variability of vegetation, land-use, water bodies and bare ground using often very generic traits to describe vegetation, the so-called Plant Functional Types (PFTs) that divides vegetation in very broad climatic (tropical, temperate, boreal), leaf kind (broad and needle) and phenological (deciduous, evergreen) classes, C3 and C4 grasses and crops whose spatial distribution was estimated from satellite data (Loveland and Belward, 1997). Within a grid, multiple PFTs compete for water and nutrients (see references in Table 1).

The structural evolution of GCMs towards the Earth System Models (ESMs), capable of a comprehensive simulation of carbon dynamics and fluxes in the, ocean and land, occurred relatively recently (Dahan, 2010; Randall et al., 2019). The land surface component of the ESMs include a prognostic representation of the biosphere that is capable to simulate plant physiological processes such as canopy and leaf processes determining radiative transfer, photosynthesis (i.e. the GPP) as well as evapotranspiration, carbon and nitrogen cycling depending of climate variables and CO₂ levels for each PFTs (Koven et al., 2013; Lawrence et al., 2019; Riley et al., 2011; Thornton et al., 2007). ESMs can estimate vegetation GPP dynamics under different climate changes scenarios providing us with the possibility of estimating the possible future gains and losses of vegetation GPP resilience.

A large number of indicators has been proposed to quantitatively measure vegetation resilience (De Keersmaecker et al., 2014a; Meyer, 2016; Scheffer et al., 2015). However, most global and regional studies estimating the impacts of climate change on vegetation productivity focus on stability i.e. the changes in GPP mean and variability due to climate extremes (Dass et al., 2016;

Kimball et al., 2009; Verduzco et al., 2018; Williams et al., 2014; Xu et al., 2020). Other studies considering future climate projections often focus on the change of mean GPP (Madani et al., 2018; Williams et al., 2014). To our knowledge no study focused specifically on GPP resilience changes yet.

In this study, we apply the annual production resilience indicator (Zampieri et al., 2019) to the GPP data generated by the new ensemble of Earth System Models simulations (ESMs, publicly accessible at <https://pcmdi.llnl.gov/CMIP6/>) included in the Sixth Coupled Models Intercomparison Project (CMIP6, <https://www.wcrp-climate.org/wgcm-cmip/wgcm-cmip6>) of the Intergovernmental Panel on Climate Change (IPCC). The annual production resilience indicator (R_p), defined as the squared mean GPP divided by its variance, allows characterizing the resilience of a production time-series with a single number (Zampieri et al., 2019). R_p is a simple indicator that offers several advantages. It is inversely proportional to the risk of production losses consistently with the ecological definition of resilience (Hollings 1973) and in principle with the engineering definition as well (Zampieri, 2021). It increases with vegetation diversity (number of species) and it accounts for memory effects, i.e., for perturbation recovery timings longer than a season (Zampieri et al., 2020c).

We quantify the changes in resilience of the GPP production in the near and far future (2021-2050 and 2051-2100) under three scenarios of socio-economical global changes, corresponding to different levels of greenhouse gases emissions and land-use, i.e. the 'Sustainability', the 'Middle of the Road' and the 'Fossil-fuel Development' scenarios. The adopted indicator and the involved ESMs simulations are described in detail in the Methods section (with additional information on the mathematical theory and properties of the resilience indicator provided in the Supplementary Material, Appendix A). The global changes in vegetation gross primary production resilience in two different periods in the future and according to three different scenarios are presented in the Results section, with reference to period 1985-2014, along with biome and country level estimates that are mainly provided in the Supplementary Material (Appendix B). Finally, in the Discussion section, the results of the study are examined in view of the ambitions of the sustainable development goals (SDGs).

Data and Methods

The definitions of resilience considered in this study refer to the ability of a system to absorb external stresses maintaining its normal functioning (ecological definition), or to recover quickly from shocks (engineering definition) (Holling, 1996, 1973; Pimm, 1984). These definitions are conceptually clear but they do not directly provide a practical way to measure resilience (Morecroft et al., 2012; Quinlan et al., 2016; Scheffer et al., 2015). In fact, a quantitative estimation of resilience requires objective methods to identify and measure the external stresses and shocks (Meyer, 2016). Also as a result of such indeterminacy, a large number of indicators was proposed to measure different aspects of resilience (De Keersmaecker et al., 2014b; Meyer, 2016; Scheffer et al., 2015; Srinivasa Rao et al., 2018).

The vegetation ability to withstand environmental perturbations (i.e. ecological resilience) can be assessed from the deviation from the seasonal climatology of vegetation above-ground biomass and proxies such as the Normalized Differential Vegetation Index (NDVI) after an environmental disturbance (Lloret et al., 2007; Van Ruijven and Berendse, 2010; Vogel et al., 2012). Such operation can be conveniently conducted after normalizing the anomalies by the mean climatological values, in order to account for the ecosystem's capacity to change (De Keersmaecker et al., 2014b).

The rate of return to the equilibrium state after a perturbation (i.e. engineering resilience) can be measured by the temporal autocorrelation of relevant vegetation variables (Dakos et al., 2012), by variance of the frequency spectrum of the anomaly time series (Zaccarelli et al., 2013), or by the spectral scaling component is given by the slope of the logarithm of the spectrum upon the

logarithm of the reverse frequency (Peng et al., 1995; Telesca et al., 2008). Up to date, none of these methods has been used to evaluate vegetation resilience at the global level and in future climate scenarios yet.

The stability of the vegetation time-series can be more easily evaluated by the absolute or normalized variance (Pimm, 1984), the latter being known as coefficient of variance. The coefficient of variance has been recently used to evaluate the effects of current climate variability on vegetation gross primary production (Chen et al., 2019; Fibbi et al., 2019; Xiao et al., 2016).

A simple and effective method, still based of a function of the mean and the variance like the coefficient of variance, but consistent with the ecological definition of resilience, was recently proposed to evaluate the production resilience of natural vegetation (Zampieri et al., 2019) and agricultural systems (Zampieri et al., 2020c). This approach is based on two assumptions (Zampieri, 2021). For annual production systems such as agriculture or natural ecosystems that are sufficiently adapted to the environmental conditions and to the local climate, it is sensible to assume that the largest disturbances are rarer compared to the “normal” conditions (assumption 1) and that the largest disturbances result in larger impacts of the annual production values (assumption 2). Under such conditions, the size of the disturbance can be univocally measured by its rareness e.g. the return period of production anomalies (T^*). It is worth noticing that T^* is the expected average number of years that pass between production losses of same size i.e. the inverse of the frequency (not to be confused with the restoring time to the equilibrium in the engineering definition of resilience). The ecological resilience can be then simply measured by T^*_{MAX} , which is the return period of the largest adverse event that the system can cope with before losing completely the production ability (Zampieri et al., 2020c).

For homogeneous agricultural production systems, T^*_{MAX} is proportional to the annual production resilience indicator, defined as:

$$(1) R_p = \mu^2 \sigma^{-2},$$

where μ is the mean and σ is the standard deviation of the annual production (Zampieri et al., 2020c; Zampieri et al., 2019).

For heterogenous production systems, R_p is linearly depending on the number of crops having the same mean production and variance, if the production fluctuations around the mean value are uncorrelated among them, and accounts consistently for different levels of cross-correlations, different mean productions and production variances characterizing diversified production systems (see Appendix A). In case the annual production resilience indicator is evaluated over a region including bare ground, the indicator is sensitive to the vegetated portion only (Zampieri et al., 2019).

Equation 1 can be easily generalized for non-stationary production systems, where the production mean and the standard deviation are not constant during the period spanned by the production time-series (Zampieri et al., 2020a). The code for handling the full problem of a diversified and non-stationary crop production systems is public and freely usable (Zampieri et al., 2020b).

In this study, R_P was computed on a large ensemble of data composed of all the climate change simulations for vegetation gross primary production available from all the Earth System Grid Federation (ESGF) portals up to 31st December 2019 for both the historical period and the climate scenarios, The climate scenarios included the ‘Sustainability (Taking the Green Road)’ (ssp126), the ‘Middle of the Road’ (ssp245) and the ‘Fossil-fuel Development (Taking the Highway)’ (ssp585) scenarios, and were evaluated considering two periods, 2021-2050 and 2051-2100, representing the near and far future periods respectively. The full list of simulations is provided in Table 1, along with the detailed reference to the land surface component of the Earth System Models.

These land surface models include a simplified representation of the biosphere with prognostic vegetation processes such as evapotranspiration, photosynthesis, carbon allocation and growth of leaves, stems and roots interacting with near surface meteorological variables such as temperature, radiation, wind and CO₂ concentration, and soil variables such as moisture, carbon and nitrogen (see references in Table 1). Therefore, in the scenarios simulation gross primary production (GPP) variability is the result of both bio–geophysical and bio–geochemical processes such as soil moisture dynamics and energy budget, permafrost thawing, atmospheric CO₂ fertilization and nitrogen limitation as well as land use changes defined as a function of the different future scenarios.

Differently from the above listed processes, Land-use changes are prescribed and are the same for all CMIP6 models (Hurtt et al., 2020). The fraction of natural vegetation changes according to the different socio-economic scenarios, but the fraction of PFTs within the grid remains constant for most models, so vegetation dynamics (i.e. spatial shifts of vegetation patterns) is not considered nor is it the internal structure of the vegetated units in terms of age of the plants' population, which is not explicitly resolved. Despite this limitation, prognostic vegetation models offer a realistic representation of the vegetation growth and of relevant variables such as the leaf area index (LAI) determining the amount of intercepted radiation, albedo and other parameters affecting the local climate as well as the carbon and nitrogen cycling.

The effects of pests and diseases are not considered, however, some of the models include the effects of peculiar abiotic disturbances such as fire (Seo and Kim, 2019). Thus, they can in principle account for two type of ecological memory (Johnstone et al., 2016; Ogle et al., 2015), which are the PFTs' adaptive response to the disturbances and the effect of the disturbances on nutrients. Memory effects linked to antecedent drought conditions (Liu et al., 2018; van der Molen et al., 2011) are well reproduced since soil moisture dynamics and the related physical feedbacks were quite well developed already in the GCMs (Seneviratne et al., 2013, 2010), which are the predecessors of the ESMs and from which ESMs inherits the representation of abiotic processes.

In general, ESMs provide a reasonable representation of the GPP response to drought (see citations in Table 1), which is, however, largely variable among models (Huang et al., 2016; Knauer et al., 2015; Orth et al., 2020). This motivates the use of a large ensemble for a robust assessment of GPP changes such as the one used here.

The annual GPP is derived by summing up monthly GPP outputs for each simulation listed in Table 1 consistently with the spatial variability of vegetation seasonality (Peano et al., 2019). This procedure is especially relevant in the Southern Hemisphere and consists of computing the annual GPP using the month with minimum GPP as boundary of the temporal window where the summation is performed, which is spatially varying, instead of using a unique time window ranging from January to December.

The spatial resolution of the ESMs is different. Therefore, the annual GPP data of each simulation is interpolated on a common 0.5 degrees regular grid with a conservative remapping method (Jones, 1999). The simulations' ensemble mean R_p is computed for each the ESMs and for each period and scenario. Finally, the overall median of the R_p changes with respect to the historical period are computed for each future period and scenario.

The robustness of the results is assessed by highlighting the areas where at least 75% of the models agree on the sign of changes (models' agreement constraint). We present the results of this analysis on global maps and by computing country level aggregates, which we discuss for the largest countries and for the countries displaying the largest changes of vegetation resilience (Table S3).

Figures S1, S2 and S3 in Supplementary Material show the ensemble model results for the GPP mean, standard deviation and resilience, which can be qualitatively compared with observed

estimates of the vegetation resilience based on remote sensing data (Zampieri et al., 2019). Figures S4 provide S5 the changes of the mean GPP and in the GPP variability, which can be compared with other studies (Dass et al., 2016; Kimball et al., 2009; Madani et al., 2018; Verduzco et al., 2018; Williams et al., 2014; Xu et al., 2020).

Distinguishing between changes in the mean and in the variability of GPP as the main drivers of changes of vegetation resilience could be useful to plan targeted adaptation strategies. In order to do so, the R_p change can be approximated by a first order 2D Taylor expansion of equation 1 as a function of the changes in the mean and in the standard deviation of the GPP as follows:

$$(2) R_{p_s} = R_{p_h} + \Delta R_p,$$

where the s stands for “scenario”, the h stands for “historical”, and Δ represents the difference between two periods.

$$(3) \Delta R_p \approx \partial R / \partial \mu \cdot \Delta \mu + \partial R / \partial \sigma \cdot \Delta \sigma$$

where ∂ is the partial derivative. By computing the derivatives and dividing both members of equation 3 by R_p one obtains:

$$(4) \Delta R_p / R_p = 2\Delta \mu / \mu - 2\Delta \sigma / \sigma.$$

Thus, an indication on the changes induced by the mean and the variability on the resilience may be obtained by comparing the projected relative changes of the mean and of the variability, using the same weight. Equation 5 provides a normalized indicator of such comparison:

$$(5) (|\Delta \mu / \mu| - |\Delta \sigma / \sigma|) / (|\Delta \mu / \mu| + |\Delta \sigma / \sigma|),$$

which varies from -1 (variability dominates) to +1 (mean dominates), which is useful to assess and compare the dominant relative changes in different locations.

Results

Future climate projections display significant changes of GPP variability resilience (Fig. 1) compared to period 1985-2014. The annual vegetation primary production resilience indicator is anticipated to generally increase in the lower emission scenarios (ssp126 and ssp245, Fig. 1 a,b,c, and d, respectively). The larger positive changes are expected to occur especially in the snow dominated bioclimatic regions (see Table S2). The amplitude and the area covered by these changes are comparatively larger in the ssp245 scenario than in the ssp126 scenario and increase with time towards the end of the 21st century (Table 2). Positive changes are also estimated for Central Africa and the Sahel regions, India and over the Himalayan Plateau. However, regions with loss of GPP resilience appear as well, especially in Brazil, China and surrounding countries of equatorial America. Under the ssp245 socio-economic scenario, the CMIP6 ESMS project resilience losses also in Mexico and the southern part of the US, the Mediterranean region, Southern Africa and Australia. This occurs not only in the far future (period 2051-2100, Fig. 1d), but also in the near future (period 2021-2050; Fig. 1c).

- Figure 1 -

Under the more moderate emission scenarios (ssp126 and ssp245), about one third of land area is going to experience an increase of vegetation annual GPP resilience over the period 2021-2050 (see Table 2). This proportion is slightly lower, about one fourth, when considering only the areas where 75% of the models agree with the sign of changes. Differently, the area with positive changes will cover almost half of the global land area (less than one third when the constraint on models' agreement is introduced) over the period 2051-2100. Regions losing resilience cover a smaller

percentage of the global area, about 10% under ssp245 in the near future period. The differences between the plain estimate and the one constrained on models' agreement become negligible for variations of resilience higher than 15% (Table 2).

The results for the ssp585 scenario stand out significantly compared to the lower emission scenarios. Broad areas with negative change (i.e. loss of vegetation GPP resilience) appear already in the period 2021-2050 (Fig. 1e) in the Amazon region, Unites States, South Canada, Western Europe, Mediterranean basin, as well as in the Middle east, Central, Western and Southern Africa, Southeast Asia and China, and Oceania. Areas with at least 5% loss of vegetation GPP resilience are projected to cover approximately one fifth of the global land (12% considering models' agreement); while areas with more than 15% losses are projected to be limited to 3%. Positive gains of vegetation GPP resilience in boreal regions are simulated to be more limited with respect to the lower emission scenarios. Gains of at least 5% are expected to cover about one fourth of the global areas (15% considering models' agreement); while areas with changes larger than 15% are limited to the 6%, similarly to the ssp126 scenario.

The severity of the projected losses is expected to further exacerbate in the period 2051-2100. In the 'Taking the Highway' scenario, less and less are the regions expected to experience gains in vegetation GPP resilience. These regions are: La Plata basin in Argentina, part of the Sahel region, Eastern Africa, Western India, North-western China and some regions along the coast of the Arctic Sea. In general, areas gaining at least 5% resilience are simulated to be limited to 14% (8% considering model agreement) of global areas, while regions with more than 15% increase of vegetation primary production resilience are limited globally to 6% of the land area. The areas losing resilience are expected to outbalance those ones increasing resilience and cover 43% (25% considering models agreement) of global land area with more than 5% resilience losses. Globally, 13% of land areas are predicted to lose more than 15 % vegetation primary production resilience.

- Figure 2 -

The GPP resilience changes can be driven either by the change in the GPP mean and by the changes in the GPP variability due to climate change (see Methods). Positive resilience changes in the near future under moderate emission scenarios are often linked to positive changes in the mean annual GPP (Fig. 2a,b,c,d,e, S4) connected to overall higher levels of atmospheric CO₂ concentration and to higher mean growing temperature in Boreal Regions. Negative resilience changes are generally associated to an increase of interannual variability of GPP (see Fig. S5). The areas affected by an increase of variability largely change across the scenarios and reach their maximum extent under the scenario ssp585 (Fig. 2e,f, S5e,f).

- Figure 3 -

Gain and losses of resilience are quantified at the national level in order to provide country-specific information for adaptation options, and possibly to support ambitious mitigation policies. This analysis is displayed in Figure 3 for the ten largest countries (and in Table S3 for all World countries). Russia is characterized by the widest gains of resilience, which could cover almost 70% of the country area in the period 2051-2100 under the ssp245 scenario. The spatial extent of areas expected to experience gains is reduced up to about 15% in the near future under the ssp585 scenario. This tendency continues towards the end of the century, under the ssp585 scenario, when also areas with GPP resilience losses start to appear. Canada shows a similar picture, but with less optimistic estimation of predicted losses largely outbalancing the gains in the 2051-2100 period under the ssp585 scenario. The USA and China display similar figures, with gains predicted to reach 20% in the low emission scenarios (ssp126 and ssp245) and losses ranging from 10% to 15% in the ssp585 over the period 2051-2100. Among the largest countries, Brazil is the one characterized by the worst projections, with the risk of losing resilience in 50% of its total territory under the ssp585 scenario at the end of the 21st Century. It is worth noting that these changes are likely to represent an underestimation as the current trend of land-use change (Freitas et al., 2018)

is only partially considered in the ESMs (Hurtt et al., 2020). Australia is estimated to undergo negligible losses, also because over desert and arid areas resilience changes are proportionally small. Nevertheless, Australia will experience comparatively large losses of resilience towards the end of the century under the ssp585 scenario. The European Union is characterized by a more stable situation with significant positive changes only under the ssp245 scenario over the period 2051-2100. India shows projections similar to the EU, but with significant areas of vegetation that both gain and lose resilience under the high emission scenario at the end of the 21st Century. Large positive and negative changes in resilience are also estimated for Argentina under the high emission scenario (2051-2100). Whether or not these compensating changes in different area are beneficial for the countries' adaptive capacity could be subject of specific follow-up investigations.

Results for the remaining World countries (see Table S3) allow identifying severe cases, such as losses of resilience higher than 15% over more than 50% of the area under the ssp585 scenario over the period 2051-2100 in Gabon, Bhutan, Venezuela, Equatorial Guinea, Malaysia, Peru, Guyana, Lebanon, Japan, Congo, Bolivia, Honduras, Zambia, South Korea, Papua Nuova Guinea and other 16 countries. Under the same scenario, the list of 'winner' countries is much shorter, with only Somalia gaining at least 15% resilience over more than 50% of its territory. Countries having the largest benefit under the ssp245 scenario at the end of the century are Russia and the ones in Northern Europe. Under the ssp126 scenario, the benefits are geographically spread into more continents. In both ssp126 and ssp245 scenarios, there are almost no countries experiencing more than 15% losses of resilience over 10% of their land.

Discussion and Conclusions

This study explores the linkages between future changes in resilience of global vegetation gross primary production (GPP) and the mitigation pathways that society can undertake to conserve and restore ecosystems and their services, on which human well-being depends. The analysis presented here highlights the world regions where there might be losses of vegetation GPP resilience as well as the countries that are subject to the most urgent necessity of improving adaptive capacity and resilience to climate-related hazards under different future climate scenarios.

The results of our analysis strongly support the SDG-13 on taking action to combat climate change and its impacts. Over anthropized area, our results are relevant for agricultural production, which is a main source of employment, livelihood and income for a large portion of population especially in developing countries (SDG-1, no poverty) as well as a main food source (SDG-2, no hunger). Our results are also relevant for the SDG-15, on the sustainable management of ecosystems and halting land degradation and biodiversity loss. Recent studies have looked at the resistance and resilience of global vegetation to short-term climate anomalies (De Keersmaecker et al., 2017) and ecosystem stability to droughts events (Huang and Xia, 2019; Ivits et al., 2012), and have highlighted how the diversity of vegetation composition and biodiversity enhances ecosystem stability (Geng et al., 2019) and the resilience of ecosystem productivity to climate extremes (Isbell et al., 2015). Enhancing biodiversity and natural capital in the most threatened areas we identified is a necessary action for the conservation and restoration of ecosystems and their services as well as to increase their stability, resilience and productivity (Cardinale et al., 2012; IPBES, 2018; Isbell et al., 2015).

The presented analysis adopts a recently proposed quantitative measure of resilience for agricultural (Zampieri et al., 2020c) and natural vegetation (Zampieri et al., 2019) productivity in order to diagnose future changes in the resilience of vegetation GPP as represented by a large ensemble of Earth System Models simulations included in the Sixth Coupled Model Intercomparison Project (CMIP6) of the Intergovernmental Panel on Climate Change (IPCC).

Our results show large differences in the changes of GPP resilience across the globe, depending on greenhouse gases concentration of the projected scenarios. Under low emission scenarios, as found in previous studies (Hubau et al., 2020), the CO₂ fertilization effect often prevail over the negative effect due global warming and to the increase of climate variability. Our results are in general agreement with the observed changes in vegetation distribution that are already observed especially in boreal regions (Keeling et al., 1996; Myneni et al., 1997). This tendency is expected to increase in the future climate scenarios, especially those with higher greenhouse gases and radiative forcing increases (Madani et al., 2018; Zampieri and Lionello, 2010; Zhang et al., 2017). However, radiation will always be a limiting factor for the vegetation adaptation at very high latitudes (Bjorkman et al., 2017; Seddon et al., 2016).

The main findings point to areas in the mid-latitudes where vegetation resilience is estimated to decrease in the higher emission scenarios, such as the Mediterranean, the mid-West in the US, Central America, part of China, Southern Africa and Australia. This tendency might compromise the stability of agricultural production and the reliability of ecosystem services provided by the natural vegetation in these regions, unless sensible adaptation actions are taken. The relevance of mitigation is most evident under the higher emission scenarios, where vegetation resilience is affected in most land areas and especially in tropical regions, where society is highly dependent on ecosystem services and more vulnerable to climatic changes.

Overall, in the scenario with lower mitigation, the areas losing vegetation resilience are more than the ones gaining resilience, jeopardizing the stability of the ecosystems structure (and of the related services). Adapting to changes in variability more than to changes in the mean production of vegetation will be critical for society and natural ecosystems in areas experiencing vegetation GPP resilience losses.

In comparison to other stability and resilience metrics, the approach adopted here offers some advantages. First of all, the annual production resilience indicator is consistent with the ecological definition of resilience by Holling (1973) because the particular combination of the mean and the variance defining it is proportional to the return period of the largest disturbance that an homogeneous system can absorb before losing the annual production (Zampieri et al., 2020c). In case the production is diversified, or the system is spatially inhomogeneous, the annual production resilience indicator increases with diversity. In particular, it increases linearly with the number of species, if their production time-series are uncorrelated among each other. In addition, if a constant portion of the area where the vegetation is computed is base ground (zero productivity), the indicator automatically adjust itself to estimate the resilience of the vegetated fraction (Zampieri et al., 2019). If the system is characterized by recovery timings larger than one year (a growing season), the value of the indicator decreases, as expected (Zampieri et al., 2020c).

However, the annual production resilience indicator has also some limitations. It does not point to the drivers determining resilience of GPP and its changes and requires relatively long data time series (see Methods and Appendix A). On the first aspect, as shown in this study, distinguishing between changes in the mean and in the variability of GPP, which are two components of the indicators, can provide additional information on the patterns behind changes. On the second aspect, using remote-sensing data, as suggested also in other large-scale studies on ecosystem stability (White et al., 2020), or long-term multi-model simulations' ensembles such as the one analysed here are favourable contexts of application.

Acknowledgments

For transparency and reproducibility, this paper uses publicly available data provided by the IPCC through the Earth System Grid Federation LLNL, CEDA, DKRZ, GFDL, IPSL, LIU, NCI and NCCS

nodes (ESGF, <https://esgf.llnl.gov/nodes.html>) and open-source software to compute the annual production resilience indicator (Zampieri et al., 2020).

Author Contributions: MZ conceived the study and drafted the paper, MZ and BG performed the analysis, PDP downloaded data and performed initial checking, all authors reviewed the manuscript and contributed to the final version.

References

Arora, V.K., Scinocca, J.F., 2016. Constraining the strength of the terrestrial CO₂ fertilization effect in the Canadian Earth system model version 4.2 (CanESM4.2). *Geosci. Model Dev.* 9, 2357–2376. <https://doi.org/10.5194/gmd-9-2357-2016>

Bastos, A., O'Sullivan, M., Ciais, P., Makowski, D., Sitch, S., Friedlingstein, P., Chevallier, F., Rödenbeck, C., Pongratz, J., Lujikx, I.T., Patra, P.K., Peylin, P., Canadell, J.G., Lauerwald, R., Li, W., Smith, N.E., Peters, W., Goll, D.S., Jain, A.K., Kato, E., Lienert, S., Lombardozzi, D.L., Haverd, V., Nabel, J.E.M.S., Poulter, B., Tian, H., Walker, A.P., Zaehle, S., 2020. Sources of Uncertainty in Regional and Global Terrestrial CO₂ Exchange Estimates. *Global Biogeochem. Cycles* 34, e2019GB006393. <https://doi.org/10.1029/2019GB006393>

Betts, R.A., Alfieri, L., Bradshaw, C., Caesar, J., Feyen, L., Friedlingstein, P., Gohar, L., Koutroulis, A., Lewis, K., Morfopoulos, C., Papadimitriou, L., Richardson, K.J., Tsanis, I., Wyser, K., 2018. Changes in climate extremes, fresh water availability and vulnerability to food insecurity projected at 1.5°C and 2°C global warming with a higher-resolution global climate model. *Philos. Trans. R. Soc. A Math. Phys. Eng. Sci.* 376, 20160452. <https://doi.org/10.1098/rsta.2016.0452>

Bjorkman, A.D., Vellend, M., Frei, E.R., Henry, G.H.R., 2017. Climate adaptation is not enough: warming does not facilitate success of southern tundra plant populations in the high Arctic. *Glob. Chang. Biol.* 23, 1540–1551. <https://doi.org/https://doi.org/10.1111/gcb.13417>

Bonan, G.B., 1998. The Land Surface Climatology of the NCAR Land Surface Model Coupled to the NCAR Community Climate Model*. *J. Clim.* 11, 1307–1326. [https://doi.org/10.1175/1520-0442\(1998\)011<1307:TLSCOT>2.0.CO;2](https://doi.org/10.1175/1520-0442(1998)011<1307:TLSCOT>2.0.CO;2)

Cardinale, B.J., Duffy, J.E., Gonzalez, A., Hooper, D.U., Perrings, C., Venail, P., Narwani, A., Mace, G.M., Tilman, D., Wardle, D.A., Kinzig, A.P., Daily, G.C., Loreau, M., Grace, J.B., Larigauderie, A., Srivastava, D.S., Naeem, S., 2012. Biodiversity loss and its impact on humanity. *Nature* 486, 59–67. <https://doi.org/10.1038/nature11148>

Chen, C., He, B., Yuan, W., Guo, L., Zhang, Y., 2019. Increasing interannual variability of global vegetation greenness. *Environ. Res. Lett.* 14, 124005. <https://doi.org/10.1088/1748-9326/ab4ffc>

Chen, Y., Ryder, J., Bastrikov, V., McGrath, M.J., Naudts, K., Otto, J., Ottlé, C., Peylin, P., Polcher, J., Valade, A., Black, A., Elbers, J.A., Moors, E., Foken, T., van Gorsel, E., Haverd, V., Heinesch, B., Tiedemann, F., Knohl, A., Launiainen, S., Loustau, D., Ogée, J., Vessala, T., Luysaert, S., 2016. Evaluating the performance of land surface model ORCHIDEE-CAN-v1.0 on water and energy flux estimation with a single- and multi-layer energy budget scheme. *Geosci. Model Dev.* 9, 2951–2972. <https://doi.org/10.5194/gmd-9-2951-2016>

Ciais, P., Reichstein, M., Viovy, N., Granier, A., Ogée, J., Allard, V., Aubinet, M., Buchmann, N.,

- Bernhofer, C., Carrara, A., Chevallier, F., De Noblet, N., Friend, A.D., Friedlingstein, P., Grünwald, T., Heinesch, B., Keronen, P., Knohl, A., Krinner, G., Loustau, D., Manca, G., Matteucci, G., Miglietta, F., Ourcival, J.M., Papale, D., Pilegaard, K., Rambal, S., Seufert, G., Soussana, J.F., Sanz, M.J., Schulze, E.D., Vesala, T., Valentini, R., 2005. Europe-wide reduction in primary productivity caused by the heat and drought in 2003. *Nature* 437, 529–533. <https://doi.org/10.1038/nature03972>
- Costanza, R., de Groot, R., Sutton, P., van der Ploeg, S., Anderson, S.J., Kubiszewski, I., Farber, S., Turner, R.K., 2014. Changes in the global value of ecosystem services. *Glob. Environ. Chang.* 26, 152–158. <https://doi.org/https://doi.org/10.1016/j.gloenvcha.2014.04.002>
- Dahan, A., 2010. Putting the Earth System in a numerical box? The evolution from climate modeling toward global change. *Stud. Hist. Philos. Sci. Part B Stud. Hist. Philos. Mod. Phys.* 41, 282–292. <https://doi.org/https://doi.org/10.1016/j.shpsb.2010.08.002>
- Dakos, V., Carpenter, S.R., Brock, W.A., Ellison, A.M., Guttal, V., Ives, A.R., Kéfi, S., Livina, V., Seekell, D.A., van Nes, E.H., Scheffer, M., 2012. Methods for Detecting Early Warnings of Critical Transitions in Time Series Illustrated Using Simulated Ecological Data. *PLoS One* 7, e41010.
- Dass, P., Rawlins, M.A., Kimball, J.S., Kim, Y., 2016. Environmental controls on the increasing GPP of terrestrial vegetation across northern Eurasia. *Biogeosciences* 13, 45–62. <https://doi.org/10.5194/bg-13-45-2016>
- De Kauwe, M.G., Kala, J., Lin, Y.-S., Pitman, A.J., Medlyn, B.E., Duursma, R.A., Abramowitz, G., Wang, Y.-P., Miralles, D.G., 2015. A test of an optimal stomatal conductance scheme within the CABLE land surface model. *Geosci. Model Dev.* 8, 431–452. <https://doi.org/10.5194/gmd-8-431-2015>
- De Keersmaecker, W., Lhermitte, S., Hill, M.J., Tits, L., Coppin, P., Somers, B., 2017. Assessment of Regional Vegetation Response to Climate Anomalies: A Case Study for Australia Using GIMMS NDVI Time Series between 1982 and 2006. *Remote Sens.* 9. <https://doi.org/10.3390/rs9010034>
- De Keersmaecker, W., Lhermitte, S., Honnay, O., Farifteh, J., Somers, B., Coppin, P., 2014a. How to measure ecosystem stability? An evaluation of the reliability of stability metrics based on remote sensing time series across the major global ecosystems. *Glob. Chang. Biol.* 20, 2149–2161. <https://doi.org/10.1111/gcb.12495>
- De Keersmaecker, W., Lhermitte, S., Honnay, O., Farifteh, J., Somers, B., Coppin, P., 2014b. How to measure ecosystem stability? An evaluation of the reliability of stability metrics based on remote sensing time series across the major global ecosystems. *Glob. Chang. Biol.* 20, 2149–2161. <https://doi.org/10.1111/gcb.12495>
- Dickinson, R.E., Shaikh, M., Bryant, R., Graumlich, L., 1998. Interactive Canopies for a Climate Model. *J. Clim.* 11, 2823–2836. [https://doi.org/10.1175/1520-0442\(1998\)011<2823:ICFACM>2.0.CO;2](https://doi.org/10.1175/1520-0442(1998)011<2823:ICFACM>2.0.CO;2)
- Dosio, A., Mentaschi, L., Fischer, E.M., Wyser, K., 2018. Extreme heat waves under 1.5 and 2 degree global warming(Supplementary data). *Environ. Res. L* 1–9.
- Fibbi, L., Moriondo, M., Chiesi, M., Bindi, M., Maselli, F., 2019. Impacts of climate change on the gross primary production of Italian forests. *Ann. For. Sci.* 76, 59. <https://doi.org/10.1007/s13595-019-0843-x>

- Forrest, M., Tost, H., Lelieveld, J., Hickler, T., 2018. Towards an advanced atmospheric chemistry-enabled ESM with dynamic land surface processes: Part I - Linking LPJ-GUESS (v4.0) with EMAC modelling system (v2.53). *Geosci. Model Dev. Discuss.* 2018, 1–21. <https://doi.org/10.5194/gmd-2018-135>
- Freitas, F.L.M., Sparovek, G., Berndes, G., Persson, U.M., Englund, O., Barretto, A., Mörtberg, U., 2018. Potential increase of legal deforestation in Brazilian Amazon after Forest Act revision. *Nat. Sustain.* 1, 665–670. <https://doi.org/10.1038/s41893-018-0171-4>
- Garrigues, S., Olioso, A., Calvet, J.C., Martin, E., Lafont, S., Moulin, S., Chanzy, A., Marloie, O., Buis, S., Desfonds, V., Bertrand, N., Renard, D., 2015a. Evaluation of land surface model simulations of evapotranspiration over a 12-year crop succession: impact of soil hydraulic and vegetation properties. *Hydrol. Earth Syst. Sci.* 19, 3109–3131. <https://doi.org/10.5194/hess-19-3109-2015>
- Garrigues, S., Olioso, A., Carrer, D., Decharme, B., Calvet, J.-C., Martin, E., Moulin, S., Marloie, O., 2015b. Impact of climate, vegetation, soil and crop management variables on multi-year ISBA-A-gs simulations of evapotranspiration over a Mediterranean crop site. *Geosci. Model Dev.* 8, 3033–3053. <https://doi.org/10.5194/gmd-8-3033-2015>
- Geng, S., Shi, P., Song, M., Zong, N., Zu, J., Zhu, W., 2019. Diversity of vegetation composition enhances ecosystem stability along elevational gradients in the Taihang Mountains, China. *Ecol. Indic.* 104, 594–603. <https://doi.org/10.1016/j.ecolind.2019.05.038>
- Gerber, S., Hedin, L.O., Oppenheimer, M., Pacala, S.W., Shevliakova, E., 2010. Nitrogen cycling and feedbacks in a global dynamic land model. *Global Biogeochem. Cycles* 24. <https://doi.org/10.1029/2008GB003336>
- Harper, A.B., Cox, P.M., Friedlingstein, P., Wiltshire, A.J., Jones, C.D., Sitch, S., Mercado, L.M., Groenendijk, M., Robertson, E., Kattge, J., Bönisch, G., Atkin, O.K., Bahn, M., Cornelissen, J., Niinemets, Ü., Onipchenko, V., Peñuelas, J., Poorter, L., Reich, P.B., Soudzilovskaia, N.A., Bodegom, P. V., 2016. Improved representation of plant functional types and physiology in the Joint UK Land Environment Simulator (JULES v4.2) using plant trait information. *Geosci. Model Dev.* 9, 2415–2440. <https://doi.org/10.5194/gmd-9-2415-2016>
- Holling, C.S., 1996. Engineering Resilience versus Ecological Resilience. *The National Academy of Sciences.*
- Holling, C.S., 1973. Resilience and stability of ecological systems. *Annu. Rev. Ecol. Syst.* 4, 1–23.
- Huang, K., Xia, J., 2019. High ecosystem stability of evergreen broadleaf forests under severe droughts. *Glob. Chang. Biol.* 25, 3494–3503. <https://doi.org/https://doi.org/10.1111/gcb.14748>
- Huang, Y., Gerber, S., Huang, T., Lichstein, J.W., 2016. Evaluating the drought response of CMIP5 models using global gross primary productivity, leaf area, precipitation, and soil moisture data. *Global Biogeochem. Cycles* 30, 1827–1846. <https://doi.org/https://doi.org/10.1002/2016GB005480>
- Hubau, W., Lewis, S.L., Phillips, O.L., Affum-Baffoe, K., Beeckman, H., Cuní-Sanchez, A., Daniels, A.K., Ewango, C.E.N., Fauset, S., Mukinzi, J.M., Sheil, D., Sonké, B., Sullivan, M.J.P., Sunderland, T.C.H., Taedoumg, H., Thomas, S.C., White, L.J.T., Abernethy, K.A., Adu-Bredu, S., Amani, C.A., Baker, T.R., Banin, L.F., Baya, F., Begne, S.K., Bennett, A.C.,

- Benedet, F., Bitariho, R., Bocko, Y.E., Boeckx, P., Boundja, P., Brienen, R.J.W., Brncic, T., Chezeaux, E., Chuyong, G.B., Clark, C.J., Collins, M., Comiskey, J.A., Coomes, D.A., Dargie, G.C., de Haulleville, T., Kamdem, M.N.D., Doucet, J.-L., Esquivel-Muelbert, A., Feldpausch, T.R., Fofanah, A., Foli, E.G., Gilpin, M., Gloor, E., Gonmadje, C., Gourlet-Fleury, S., Hall, J.S., Hamilton, A.C., Harris, D.J., Hart, T.B., Hockemba, M.B.N., Hladik, A., Ifo, S.A., Jeffery, K.J., Jucker, T., Yakusu, E.K., Kearsley, E., Kenfack, D., Koch, A., Leal, M.E., Levesley, A., Lindsell, J.A., Lisingo, J., Lopez-Gonzalez, G., Lovett, J.C., Makana, J.-R., Malhi, Y., Marshall, A.R., Martin, J., Martin, E.H., Mbayu, F.M., Medjibe, V.P., Mihindou, V., Mitchard, E.T.A., Moore, S., Munishi, P.K.T., Bengone, N.N., Ojo, L., Ondo, F.E., Peh, K.S.-H., Pickavance, G.C., Poulsen, A.D., Poulsen, J.R., Qie, L., Reitsma, J., Rovero, F., Swaine, M.D., Talbot, J., Taplin, J., Taylor, D.M., Thomas, D.W., Toirambe, B., Mukendi, J.T., Tuagben, D., Umunay, P.M., van der Heijden, G.M.F., Verbeeck, H., Vleminckx, J., Willcock, S., Wöll, H., Woods, J.T., Zomagho, L., 2020. Asynchronous carbon sink saturation in African and Amazonian tropical forests. *Nature* 579, 80–87. <https://doi.org/10.1038/s41586-020-2035-0>
- Hurt, G.C., Chini, L., Sahajpal, R., Frolking, S., Bodirsky, B.L., Calvin, K., Doelman, J.C., Fisk, J., Fujimori, S., Goldewijk, K.K., Hasegawa, T., Havlik, P., Heinemann, A., Humpenöder, F., Jungclaus, J., Kaplan, J., Kennedy, J., Kristzin, T., Lawrence, D., Lawrence, P., Ma, L., Mertz, O., Pongratz, J., Popp, A., Poulter, B., Riahi, K., Shevliakova, E., Stehfest, E., Thornton, P., Tubiello, F.N., van Vuuren, D.P., Zhang, X., 2020. Harmonization of Global Land-Use Change and Management for the Period 850–2100 (LUH2) for CMIP6. *Geosci. Model Dev. Discuss.* 2020, 1–65. <https://doi.org/10.5194/gmd-2019-360>
- IPBES, 2018. The IPBES assessment report on land degradation and restoration. Secretariat of the Intergovernmental Science-Policy Platform on Biodiversity and Ecosystem Services, Bonn, Germany.
- Isbell, F., Craven, D., Connolly, J., Loreau, M., Schmid, B., Beierkuhnlein, C., Bezemer, T.M., Bonin, C., Bruehlheide, H., de Luca, E., Ebeling, A., Griffin, J.N., Guo, Q., Hautier, Y., Hector, A., Jentsch, A., Kreyling, J., Lanta, V., Manning, P., Meyer, S.T., Mori, A.S., Naeem, S., Niklaus, P.A., Polley, H.W., Reich, P.B., Roscher, C., Seabloom, E.W., Smith, M.D., Thakur, M.P., Tilman, D., Tracy, B.F., van der Putten, W.H., van Ruijven, J., Weigelt, A., Weisser, W.W., Wilsey, B., Eisenhauer, N., 2015. Biodiversity increases the resistance of ecosystem productivity to climate extremes. *Nature* 526, 574–577. <https://doi.org/10.1038/nature15374>
- Ito, A., Inatomi, M., 2011. Water-Use Efficiency of the Terrestrial Biosphere: A Model Analysis Focusing on Interactions between the Global Carbon and Water Cycles. *J. Hydrometeorol.* 13, 681–694. <https://doi.org/10.1175/JHM-D-10-05034.1>
- Ivits, E., Cherlet, M., Tóth, G., Sommer, S., Mehl, W., Vogt, J., Micale, F., 2012. Combining satellite derived phenology with climate data for climate change impact assessment. *Glob. Planet. Change* 88–89, 85–97. <https://doi.org/https://doi.org/10.1016/j.gloplacha.2012.03.010>
- Johnstone, J.F., Allen, C.D., Franklin, J.F., Frelich, L.E., Harvey, B.J., Higuera, P.E., Mack, M.C., Meentemeyer, R.K., Metz, M.R., Perry, G.L.W., Schoennagel, T., Turner, M.G., 2016. Changing disturbance regimes, ecological memory, and forest resilience. *Front. Ecol. Environ.* 14, 369–378. <https://doi.org/https://doi.org/10.1002/fee.1311>
- Jones, P.W., 1999. First- and Second-Order Conservative Remapping Schemes for Grids in Spherical Coordinates. *Mon. Weather Rev.* 127, 2204–2210. [https://doi.org/10.1175/1520-0493\(1999\)127<2204:FASOCR>2.0.CO;2](https://doi.org/10.1175/1520-0493(1999)127<2204:FASOCR>2.0.CO;2)

- Keeling, C.D., Chin, J.F.S., Whorf, T.P., 1996. Increased activity of northern vegetation inferred from atmospheric CO₂ measurements. *Nature* 382, 146–149. <https://doi.org/10.1038/382146a0>
- Kimball, J.S., Zhao, M., McGuire, A.D., Heinsch, F.A., Clein, J., Calef, M., Jolly, W.M., Kang, S., Euskirchen, S.E., McDonald, K.C., Running, S.W., 2009. Recent Climate-Driven Increases in Vegetation Productivity for the Western Arctic: Evidence of an Acceleration of the Northern Terrestrial Carbon Cycle. *Earth Interact.* 11, 1–30. <https://doi.org/10.1175/EI180.1>
- Knauer, J., Werner, C., Zaehle, S., 2015. Evaluating stomatal models and their atmospheric drought response in a land surface scheme: A multibiome analysis. *J. Geophys. Res. Biogeosciences* 120, 1894–1911. <https://doi.org/10.1002/2015JG003114>
- Koven, C.D., Riley, W.J., Subin, Z.M., Tang, J.Y., Torn, M.S., Collins, W.D., Bonan, G.B., Lawrence, D.M., Swenson, S.C., 2013. The effect of vertically resolved soil biogeochemistry and alternate soil C and N models on C dynamics of CLM4. *Biogeosciences* 10, 7109–7131. <https://doi.org/10.5194/bg-10-7109-2013>
- Lawrence, D.M., Fisher, R.A., Koven, C.D., Oleson, K.W., Swenson, S.C., Bonan, G., Collier, N., Ghimire, B., van Kampenhout, L., Kennedy, D., Kluzek, E., Lawrence, P.J., Li, F., Li, H., Lombardozi, D., Riley, W.J., Sacks, W.J., Shi, M., Vertenstein, M., Wieder, W.R., Xu, C., Ali, A.A., Badger, A.M., Bisht, G., van den Broeke, M., Brunke, M.A., Burns, S.P., Buzan, J., Clark, M., Craig, A., Dahlin, K., Drewniak, B., Fisher, J.B., Flanner, M., Fox, A.M., Gentine, P., Hoffman, F., Keppel-Aleks, G., Knox, R., Kumar, S., Lenaerts, J., Leung, L.R., Lipscomb, W.H., Lu, Y., Pandey, A., Pelletier, J.D., Perket, J., Randerson, J.T., Ricciuto, D.M., Sanderson, B.M., Slater, A., Subin, Z.M., Tang, J., Thomas, R.Q., Val Martin, M., Zeng, X., 2019. The Community Land Model Version 5: Description of New Features, Benchmarking, and Impact of Forcing Uncertainty. *J. Adv. Model. Earth Syst.* 11, 4245–4287. <https://doi.org/10.1029/2018MS001583>
- Liu, L., Zhang, Y., Wu, S., Li, S., Qin, D., 2018. Water memory effects and their impacts on global vegetation productivity and resilience. *Sci. Rep.* 8, 2962. <https://doi.org/10.1038/s41598-018-21339-4>
- Lloret, F., Lobo, A., Estevan, H., Maisongrande, P., Vayreda, J., Terradas, J., 2007. Woody Plant Richness and NDVI Response to Drought Events in Catalanian (Northeastern Spain) Forests. *Ecology* 88, 2270–2279.
- Lotka, A.J., 1920. Analytical Note on Certain Rhythmic Relations in Organic Systems. *Proc. Natl. Acad. Sci.* 6, 410–415. <https://doi.org/10.1073/pnas.6.7.410>
- Loveland, T.R., Belward, A.S., 1997. The IGBP-DIS global 1km land cover data set, DISCover: First results. *Int. J. Remote Sens.* 18, 3289–3295. <https://doi.org/10.1080/014311697217099>
- Madani, N., Kimball, J.S., Ballantyne, A.P., Affleck, D.L.R., van Bodegom, P.M., Reich, P.B., Kattge, J., Sala, A., Nazeri, M., Jones, M.O., Zhao, M., Running, S.W., 2018. Future global productivity will be affected by plant trait response to climate. *Sci. Rep.* 8, 2870. <https://doi.org/10.1038/s41598-018-21172-9>
- MAE, 2005. Millennium Ecosystem Assessment. *Ecosystems and Human Well-Being: Synthesis*. Washington DC.
- Meyer, K., 2016. A mathematical review of resilience in ecology. *Nat. Resour. Model.* 29, 339–

352. <https://doi.org/10.1111/nrm.12097>

- Mitchell, J.F.B., Johns, T.C., Gregory, J.M., Tett, S.F.B., 1995. Climate response to increasing levels of greenhouse gases and sulphate aerosols. *Nature* 376, 501–504. <https://doi.org/10.1038/376501a0>
- Moore, J.C., de Ruiter, P.C., Hunt, H.W., 1993. Influence of Productivity on the Stability of Real and Model Ecosystems. *Science* (80-). 261, 906–908. <https://doi.org/10.1126/science.261.5123.906>
- Morecroft, M.D., Crick, H.Q.P., Duffield, S.J., Macgregor, N.A., 2012. Resilience to climate change: translating principles into practice. *J. Appl. Ecol.* 49, 547–551. <https://doi.org/10.1111/j.1365-2664.2012.02136.x>
- Murphy, J.M., 1995. Transient Response of the Hadley Centre Coupled Ocean-Atmosphere Model to Increasing Carbon Dioxide. Part III: Analysis of Global-Mean Response Using Simple Models. *J. Clim.* 8, 496–514. [https://doi.org/10.1175/1520-0442\(1995\)008<0496:TROTHC>2.0.CO;2](https://doi.org/10.1175/1520-0442(1995)008<0496:TROTHC>2.0.CO;2)
- Myneni, R.B., Keeling, C.D., Tucker, C.J., Asrar, G., Nemani, R.R., 1997. Increased plant growth in the northern high latitudes from 1981 to 1991. *Nature* 386, 698–702. <https://doi.org/10.1038/386698a0>
- Naumann, G., Alfieri, L., Wyser, K., Mentaschi, L., Betts, R.A., Carrao, H., Spinoni, J., Vogt, J., Feyen, L., 2018. Global Changes in Drought Conditions under Different Levels of Warming. *Geophys. Res. Lett.* <https://doi.org/10.1002/2017GL076521>
- Ogle, K., Barber, J.J., Barron-Gafford, G.A., Bentley, L.P., Young, J.M., Huxman, T.E., Loik, M.E., Tissue, D.T., 2015. Quantifying ecological memory in plant and ecosystem processes. *Ecol. Lett.* 18, 221–235. <https://doi.org/https://doi.org/10.1111/ele.12399>
- Oliver, T.H., Heard, M.S., Isaac, N.J.B., Roy, D.B., Procter, D., Eigenbrod, F., Freckleton, R., Hector, A., Orme, C.D.L., Petchey, O.L., Proença, V., Raffaelli, D., Suttle, K.B., Mace, G.M., Martín-López, B., Woodcock, B.A., Bullock, J.M., 2015. Biodiversity and Resilience of Ecosystem Functions. *Trends Ecol. Evol.* 30, 673–684. <https://doi.org/https://doi.org/10.1016/j.tree.2015.08.009>
- Orth, R., Destouni, G., Jung, M., Reichstein, M., 2020. Large-scale biospheric drought response intensifies linearly with drought duration in arid regions. *Biogeosciences* 17, 2647–2656. <https://doi.org/10.5194/bg-17-2647-2020>
- Peano, D., Materia, S., Collalti, A., Alessandri, A., Anav, A., Bombelli, A., Gualdi, S., 2019. Global Variability of Simulated and Observed Vegetation Growing Season. *J. Geophys. Res. Biogeosciences* 124, 3569–3587. <https://doi.org/10.1029/2018JG004881>
- Peng, C. -K., Havlin, S., Stanley, H.E., Goldberger, A.L., 1995. Quantification of scaling exponents and crossover phenomena in nonstationary heartbeat time series. *Chaos An Interdiscip. J. Nonlinear Sci.* 5, 82–87. <https://doi.org/10.1063/1.166141>
- Peters, W., van der Velde, I.R., van Schaik, E., Miller, J.B., Ciais, P., Duarte, H.F., van der Laan-Luijkx, I.T., van der Molen, M.K., Scholze, M., Schaefer, K., Vidale, P.L., Verhoef, A., Wårlind, D., Zhu, D., Tans, P.P., Vaughn, B., White, J.W.C., 2018. Increased water-use efficiency and reduced CO₂ uptake by plants during droughts at a continental-scale. *Nat. Geosci.* 11, 744–748. <https://doi.org/10.1038/s41561-018-0212-7>

- Pimm, S.L., 1984. The complexity and stability of ecosystems. *Nature* 307, 321–326.
<https://doi.org/10.1038/307321a0>
- Pokhrel, Y., Felfelani, F., Satoh, Y., Boulange, J., Burek, P., Gädeke, A., Gerten, D., Gosling, S.N., Grillakis, M., Gudmundsson, L., Hanasaki, N., Kim, H., Koutroulis, A., Liu, J., Papadimitriou, L., Schewe, J., Müller Schmied, H., Stacke, T., Telteu, C.-E., Thiery, W., Veldkamp, T., Zhao, F., Wada, Y., 2021. Global terrestrial water storage and drought severity under climate change. *Nat. Clim. Chang.* <https://doi.org/10.1038/s41558-020-00972-w>
- Quinlan, A.E., Berbés-Blázquez, M., Haider, L.J., Peterson, G.D., 2016. Measuring and assessing resilience: broadening understanding through multiple disciplinary perspectives. *J. Appl. Ecol.* 53, 677–687. <https://doi.org/10.1111/1365-2664.12550>
- Randall, D.A., Bitz, C.M., Danabasoglu, G., Denning, A.S., Gent, P.R., Gettelman, A., Griffies, S.M., Lynch, P., Morrison, H., Pincus, R., Thuburn, J., 2019. 100 Years of Earth System Model Development. *Meteorol. Monogr.* 59, 12.1–12.66.
<https://doi.org/10.1175/AMSMONOGRAPHS-D-18-0018.1>
- Raupach, M.R., Marland, G., Ciais, P., Le Quéré, C., Canadell, J.G., Klepper, G., Field, C.B., 2007. Global and regional drivers of accelerating CO₂ emissions. *Proc. Natl. Acad. Sci.* 104, 10288–10293. <https://doi.org/10.1073/pnas.0700609104>
- Reick, C.H., Raddatz, T., Brovkin, V., Gayler, V., 2013. Representation of natural and anthropogenic land cover change in MPI-ESM. *J. Adv. Model. Earth Syst.* 5, 459–482.
<https://doi.org/10.1002/jame.20022>
- Richmond, A., Kaufmann, R.K., Myneni, R.B., 2007. Valuing ecosystem services: A shadow price for net primary production. *Ecol. Econ.* 64, 454–462.
<https://doi.org/https://doi.org/10.1016/j.ecolecon.2007.03.009>
- Riley, W.J., Subin, Z.M., Lawrence, D.M., Swenson, S.C., Torn, M.S., Meng, L., Mahowald, N.M., Hess, P., 2011. Barriers to predicting changes in global terrestrial methane fluxes: analyses using CLM4Me, a methane biogeochemistry model integrated in CESM. *Biogeosciences* 8, 1925–1953. <https://doi.org/10.5194/bg-8-1925-2011>
- Sage, R.F., Kubian, D.S., 2007. The temperature response of C₃ and C₄ photosynthesis. *Plant. Cell Environ.* 30, 1086–1106. <https://doi.org/10.1111/j.1365-3040.2007.01682.x>
- Sausen, R., Barthel, K., Hasselmann, K., 1988. Coupled ocean-atmosphere models with flux correction. *Clim. Dyn.* 2, 145–163. <https://doi.org/10.1007/BF01053472>
- Scheffer, M., Carpenter, S.R., Dakos, V., van Nes, E.H., 2015. Generic Indicators of Ecological Resilience: Inferring the Chance of a Critical Transition. *Annu. Rev. Ecol. Evol. Syst.* 46, 145–167. <https://doi.org/10.1146/annurev-ecolsys-112414-054242>
- Seddon, A.W.R., Macias-Fauria, M., Long, P.R., Benz, D., Willis, K.J., 2016. Sensitivity of global terrestrial ecosystems to climate variability. *Nature* 531, 229.
- Seddon, N., Turner, B., Berry, P., Chausson, A., Girardin, C.A.J., 2019. Grounding nature-based climate solutions in sound biodiversity science. *Nat. Clim. Chang.* 9, 84–87.
<https://doi.org/10.1038/s41558-019-0405-0>
- Seneviratne, S.I., Corti, T., Davin, E.L., Hirschi, M., Jaeger, E.B., Lehner, I., Orlowsky, B.,

- Teuling, A.J., 2010. Investigating soil moisture–climate interactions in a changing climate: A review. *Earth-Science Rev.* 99, 125–161. <https://doi.org/https://doi.org/10.1016/j.earscirev.2010.02.004>
- Seneviratne, S.I., Wilhelm, M., Stanelle, T., van den Hurk, B., Hagemann, S., Berg, A., Cheruy, F., Higgins, M.E., Meier, A., Brovkin, V., Claussen, M., Ducharne, A., Dufresne, J.-L., Findell, K.L., Ghattas, J., Lawrence, D.M., Malyshev, S., Rummukainen, M., Smith, B., 2013. Impact of soil moisture-climate feedbacks on CMIP5 projections: First results from the GLACE-CMIP5 experiment. *Geophys. Res. Lett.* 40, 5212–5217. <https://doi.org/https://doi.org/10.1002/grl.50956>
- Seo, H., Kim, Y., 2019. Interactive impacts of fire and vegetation dynamics on global carbon and water budget using Community Land Model version 4.5. *Geosci. Model Dev.* 12, 457–472. <https://doi.org/10.5194/gmd-12-457-2019>
- Srinivasa Rao, C., Kareemulla, K., Krishnan, P., Murthy, G.R.K., Ramesh, P., Ananthan, P.S., Joshi, P.K., 2018. Agro-ecosystem based sustainability indicators for climate resilient agriculture in India: A conceptual framework. *Ecol. Indic.* 0–1. <https://doi.org/10.1016/j.ecolind.2018.06.038>
- Stuart-Haëntjens, E., De Boeck, H.J., Lemoine, N.P., Mänd, P., Kröel-Dulay, G., Schmidt, I.K., Jentsch, A., Stampfli, A., Anderegg, W.R.L., Bahn, M., Kreyling, J., Wohlgemuth, T., Lloret, F., Classen, A.T., Gough, C.M., Smith, M.D., 2018. Mean annual precipitation predicts primary production resistance and resilience to extreme drought. *Sci. Total Environ.* 636, 360–366. <https://doi.org/https://doi.org/10.1016/j.scitotenv.2018.04.290>
- Telesca, L., Lasaponara, R., Lanorte, A., 2008. Intra-annual dynamical persistent mechanisms in mediterranean ecosystems revealed SPOT-VEGETATION time series. *Ecol. Complex.* 5, 151–156. <https://doi.org/https://doi.org/10.1016/j.ecocom.2007.10.001>
- Thornton, P.E., Lamarque, J.-F., Rosenbloom, N.A., Mahowald, N.M., 2007. Influence of carbon-nitrogen cycle coupling on land model response to CO₂ fertilization and climate variability. *Global Biogeochem. Cycles* 21. <https://doi.org/https://doi.org/10.1029/2006GB002868>
- Toreti, A., Belward, A., Perez-Dominguez, I., Naumann, G., Luterbacher, J., Cronie, O., Seguini, L., Manfron, G., Lopez-Lozano, R., Baruth, B., van den Berg, M., Dentener, F., Ceglar, A., Chatzopoulos, T., Zampieri, M., 2019. The Exceptional 2018 European Water Seesaw Calls for Action on Adaptation. *Earth's Futur.* 7, 652–663. <https://doi.org/10.1029/2019EF001170>
- Toreti, A., Deryng, D., Tubiello, F.N., Müller, C., Kimball, B.A., Moser, G., Boote, K., Asseng, S., Pugh, T.A.M., Vanuytrecht, E., Pleijel, H., Webber, H., Durand, J.-L., Dentener, F., Ceglar, A., Wang, X., Badeck, F., Lecerf, R., Wall, G.W., van den Berg, M., Hoegy, P., Lopez-Lozano, R., Zampieri, M., Galmarini, S., O'Leary, G.J., Manderscheid, R., Mencos Contreras, E., Rosenzweig, C., 2020. Narrowing uncertainties in the effects of elevated CO₂ on crops. *Nat. Food* 1, 775–782. <https://doi.org/10.1038/s43016-020-00195-4>
- United Nations, 2016. Report of the Inter-Agency and Expert Group on Sustainable Development Goal Indicators. New York. [https://doi.org/\(E/CN.3/2016/2/Rev.1\)](https://doi.org/(E/CN.3/2016/2/Rev.1))
- van der Molen, M.K., Dolman, A.J., Ciais, P., Eglin, T., Gobron, N., Law, B.E., Meir, P., Peters, W., Phillips, O.L., Reichstein, M., Chen, T., Dekker, S.C., Doubková, M., Friedl, M.A., Jung, M., van den Hurk, B.J.J.M., de Jeu, R.A.M., Kruijt, B., Ohta, T., Rebel, K.T., Plummer, S., Seneviratne, S.I., Sitch, S., Teuling, A.J., van der Werf, G.R., Wang, G., 2011. Drought and ecosystem carbon cycling. *Agric. For. Meteorol.* 151, 765–773.

<https://doi.org/https://doi.org/10.1016/j.agrformet.2011.01.018>

- Van Ruijven, J., Berendse, F., 2010. Diversity enhances community recovery, but not resistance, after drought. *J. Ecol.* 98, 81–86. <https://doi.org/https://doi.org/10.1111/j.1365-2745.2009.01603.x>
- Vargas, L., Willemsen, L., Hein, L., 2019. Assessing the Capacity of Ecosystems to Supply Ecosystem Services Using Remote Sensing and An Ecosystem Accounting Approach. *Environ. Manage.* 63, 1–15. <https://doi.org/10.1007/s00267-018-1110-x>
- Verduzco, V.S., Vivoni, E.R., Yépez, E.A., Rodríguez, J.C., Watts, C.J., Tarin, T., Garatuza-Payán, J., Robles-Morua, A., Ivanov, V.Y., 2018. Climate Change Impacts on Net Ecosystem Productivity in a Subtropical Shrubland of Northwestern México. *J. Geophys. Res. Biogeosciences* 123, 688–711. <https://doi.org/10.1002/2017JG004361>
- Vogel, A., Scherer-Lorenzen, M., Weigelt, A., 2012. Grassland Resistance and Resilience after Drought Depends on Management Intensity and Species Richness. *PLoS One* 7, e36992.
- Volodin, E.M., Mortikov, E. V, Kostykin, S. V, Galin, V.Y., Lykossov, V.N., Gritsun, A.S., Diansky, N.A., Gusev, A. V, Iakovlev, N.G., 2017. Simulation of the present-day climate with the climate model INMCM5. *Clim. Dyn.* 49, 3715–3734. <https://doi.org/10.1007/s00382-017-3539-7>
- Volterra, V., 1926. Variazioni e fluttuazioni del numero d'individui in specie animali conviventi. *Mem. Acad. Lincei Roma* 2, 31–113.
- White, H.J., Gaul, W., Sadykova, D., León-Sánchez, L., Caplat, P., Emmerson, M.C., Yearsley, J.M., 2020. Quantifying large-scale ecosystem stability with remote sensing data. *Remote Sens. Ecol. Conserv.* 6, 354–365. <https://doi.org/https://doi.org/10.1002/rse2.148>
- Williams, I.N., Torn, M.S., Riley, W.J., Wehner, M.F., 2014. Impacts of climate extremes on gross primary production under global warming. *Environ. Res. Lett.* 9, 94011. <https://doi.org/10.1088/1748-9326/9/9/094011>
- Xiao, J., Liu, S., Stoy, P.C., 2016. Preface: Impacts of extreme climate events and disturbances on carbon dynamics. *Biogeosciences* 13, 3665–3675. <https://doi.org/10.5194/bg-13-3665-2016>
- Xu, K., Wang, X., Jiang, C., Sun, O.J., 2020. Assessing the vulnerability of ecosystems to climate change based on climate exposure, vegetation stability and productivity. *For. Ecosyst.* 7, 23. <https://doi.org/10.1186/s40663-020-00239-y>
- Zaccarelli, N., Li, B.-L., Petrosillo, I., Zurlini, G., 2013. Order and disorder in ecological time-series: Introducing normalized spectral entropy. *Ecol. Indic.* 28, 22–30. <https://doi.org/https://doi.org/10.1016/j.ecolind.2011.07.008>
- Zampieri, M., 2021. Reconciling the ecological and engineering definitions of resilience. *Ecosphere*. <https://doi.org/https://doi.org/10.1002/ecs2.3375>
- Zampieri, M., Grizzetti, B., Meroni, M., Scoccimarro, E., Vrieling, A., Naumann, G., Toreti, A., 2019. Annual Green Water Resources and Vegetation Resilience Indicators: Definitions, Mutual Relationships, and Future Climate Projections. *Remote Sens.* 11, 2708. <https://doi.org/10.3390/rs11222708>

- Zampieri, M., Lionello, P., 2010. Simple statistical approach for computing land cover types and potential natural vegetation. *Clim. Res.* 41. <https://doi.org/10.3354/cr00846>
- Zampieri, M., Toreti, A., Ceglar, A., de Palma, P., Chatzopoulos, T., 2020. Analysing the resilience of the European commodity production system with PyResPro, the Python Production Resilience package. *arXiv*.
- Zampieri, Matteo, Toreti, A., Ceglar, A., Naumann, G., Turco, M., Tebaldi, C., 2020a. Climate resilience of the top ten wheat producers in the Mediterranean and the Middle East. *Reg. Environ. Chang.* 20, 41. <https://doi.org/10.1007/s10113-020-01622-9>
- Zampieri, Matteo, Toreti, A., Ceglar, A., Palma, P. De, Chatzopoulos, T., 2020b. Analysing the resilience of the European commodity production system with PyResPro, the Python Production Resilience package. *arXiv* 2006.08976.
- Zampieri, Matteo, Weissteiner, C.J., Grizzetti, B., Toreti, A., van den Berg, M., Dentener, F., 2020c. Estimating resilience of crop production systems: From theory to practice. *Sci. Total Environ.* 735, 139378. <https://doi.org/https://doi.org/10.1016/j.scitotenv.2020.139378>
- Zhang, Z., Zhang, R., Cescatti, A., Wohlfahrt, G., Buchmann, N., Zhu, J., Chen, G., Moyano, F., Pumpanen, J., Hirano, T., Takagi, K., Merbold, L., 2017. Effect of climate warming on the annual terrestrial net ecosystem CO₂ exchange globally in the boreal and temperate regions. *Sci. Rep.* 7, 3108. <https://doi.org/10.1038/s41598-017-03386-5>

Figures and Tables

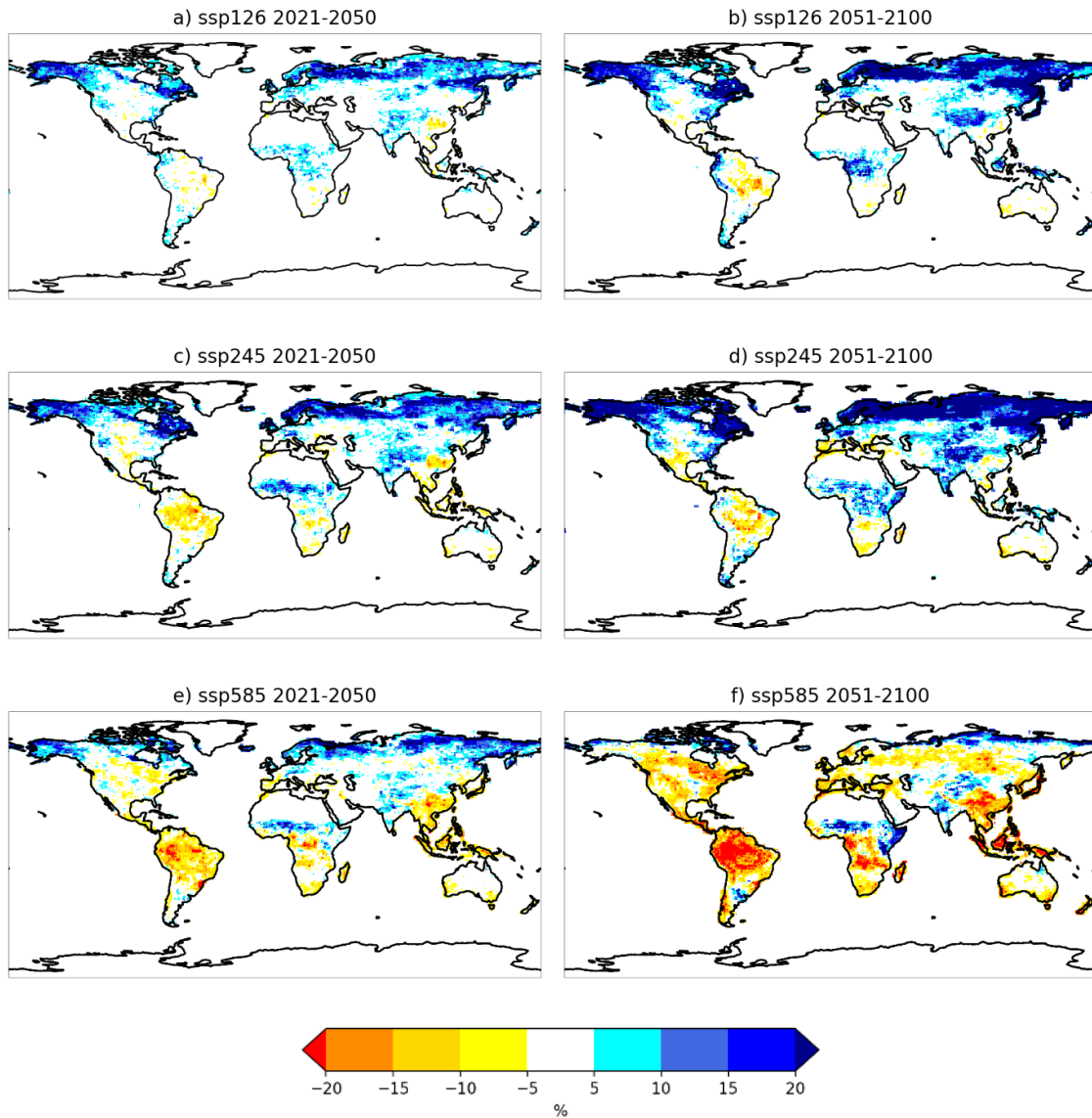


Figure 1. Global changes of annual gross primary production resilience (R_p) computed from an ensemble of 16 Earth System Models (ESMs) simulations under ssp126 (panels a and b), ssp245 (panels c and d), and ssp585 (panels e and f) CMIP6 scenarios in the periods 2021-2050 (panels a, c, and e) and 2051-2100 (panels b, d, and f) compared to the period 1985-2014.

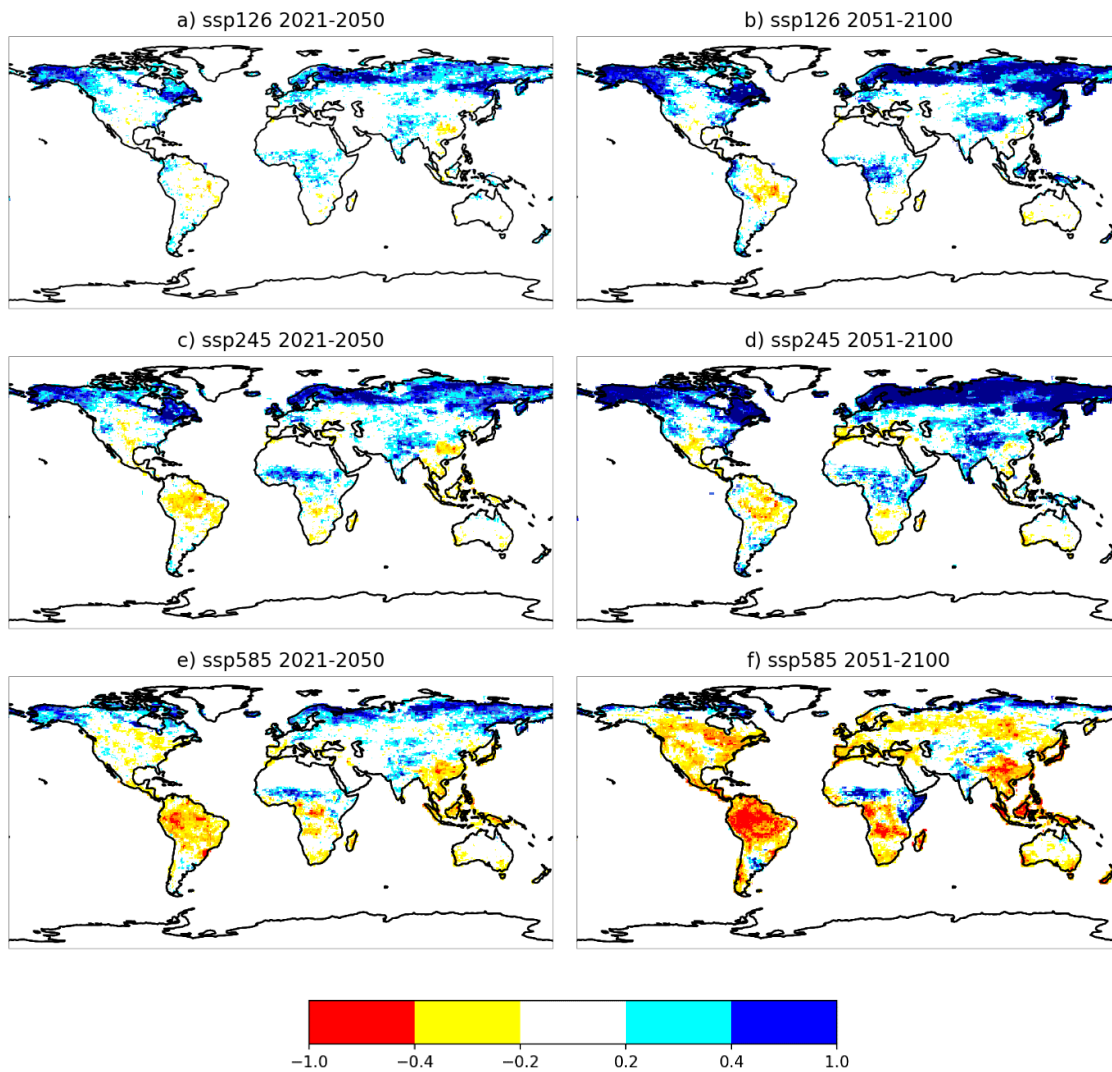


Figure 2. Ensemble mean share of the two factors triggering changes in the vegetation annual production resilience indicator (as from eq. 5, see Methods). Positive values (light and dark blue areas) point to changes in the resilience indicator mainly due to changes in the mean GPP. Negative values (red and yellow areas) are associated with grid points where the changes in the resilience indicator are mainly driven by changes in the GPP variability.

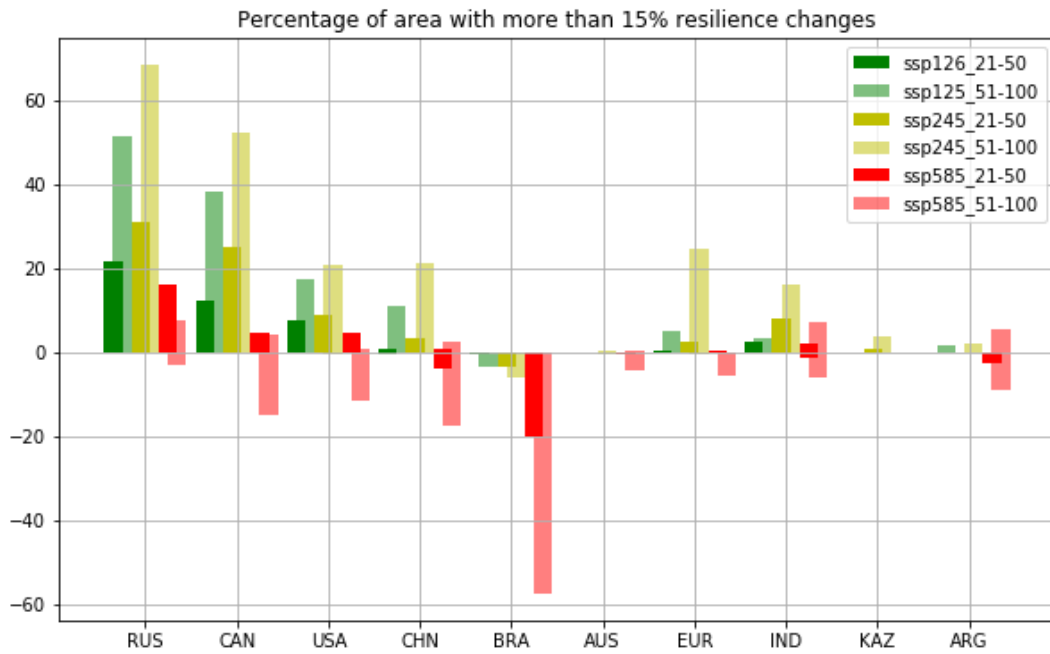


Figure 3. Percentages of area with more than 15% annual GPP resilience change for the ten wider countries, Russia (RUS), Canada (CAN), the United States of America (USA), China (CHN), Brazil (BRA), Australia (AUS), the European Union (EUR), India (IND), Kazakhstan (KAZ), and Argentina (ARG). Negative values refer to the percentage of areas with negative GPP resilience changes.

Table 1. Earth System Model (ESMs) simulations producing the annual gross primary production (GPP) data used in this study; with information on: modules delegated to the representation of land surface processes and GPP simulations (and associated reference publications); number of simulations available up to 31st December 2019 for the historical period and for ssp126, ssp245 and ssp585 future scenarios.

ESM	Land Model	historical	ssp126	ssp245	ssp585
ACCESS-ESM-5	CABLE w/Carbon cycle (De Kauwe et al., 2015)	1	1	1	1
CESM2-WACCM	CLM5 (Lawrence et al., 2019)	3	1	1	1
CESM2	CLM5 (Lawrence et al., 2019)	10	2	3	2
CNRM-CM6-1	ISBA with fixed LAI monthly climatology (Garrigues et al., 2015a, 2015b)	30	1	6	6
CNRM-ESM-1	ISBA with interactive LAI (Garrigues et al., 2015b, 2015a)	7	1	5	5
CanESM5-CanOE	CLASS-CTEM (Arora and Scinocca, 2016)	3	3	3	3
CanESM5	CLASS-CTEM (Arora and Scinocca, 2016)	50	50	50	50
EC-Earth3-Veg	LPJ-GUESS v4 (Forrest et al., 2018)	4	3	3	3
INM-CM4-8	no name (Volodin et al., 2017)	1	1	1	1
INM-CM5-0	no name ⁵	10	1	1	1
IPSL-CM6A-LR	ORCHIDEE (Chen et al., 2016)	30	1	9	6
MIROC-ES2L	VISIT-e (Ito and Inatomi, 2011)	3	1	1	1
MPI-ESM1-2-HR	JSBACH (Reick et al., 2013)	10	2	2	2
MPI-ESM2-2-LR	JSBACH (Reick et al., 2013)	10	10	10	10
NorESM2-LM	GFDL-LM3.0 (Gerber et al., 2010)	3	1	3	1
UKEMS1-0-LL	JULES (Harper et al., 2016)	19	5	4	5

Table 2. Fraction of global land area where the relative resilience indicator ($\Delta R_p/R_p$) exceeds different thresholds (5%; 10%; 15%; 20%) in the simulation ensemble median. The first estimation (third and fourth columns) considers all areas displaying changes larger than the thresholds. A second estimate (fifth and sixth columns) is restricted to the areas where at least the 75% of the models agree on the sign of changes.

		Fraction of land area with changing resilience		Fraction of land area considering 75% models' agreement	
<i>Period</i>	<i>Scenario</i>	$\Delta R_p/R_p > 5\%$	$\Delta R_p/R_p < 5\%$	$\Delta R_p/R_p > 5\%$	$\Delta R_p/R_p < 5\%$
2021-2050	ssp126	31%	2%	25%	1%
	ssp245	35%	9%	27%	4%
	ssp585	24%	21%	15%	12%
2051-2100	ssp126	41%	3%	36%	1%
	ssp245	48%	8%	27%	4%
	ssp585	14%	43%	8%	25%
		$\Delta R_p/R_p > 10\%$	$\Delta R_p/R_p < 10\%$	$\Delta R_p/R_p > 10\%$	$\Delta R_p/R_p < 10\%$
2021-2050	ssp126	15%	0%	13%	0%
	ssp245	21%	2%	19%	1%
	ssp585	12%	8%	9%	6%
2051-2100	ssp126	27%	0%	26%	0%
	ssp245	35%	2%	30%	1%
	ssp585	8%	27%	6%	20%
		$\Delta R_p/R_p > 15\%$	$\Delta R_p/R_p < 15\%$	$\Delta R_p/R_p > 15\%$	$\Delta R_p/R_p < 15\%$
2021-2050	ssp126	7%	0%	7%	0%
	ssp245	12%	0%	11%	0%
	ssp585	6%	3%	5%	2%
2051-2100	ssp126	20%	0%	19%	0%
	ssp245	26%	0%	25%	0%
	ssp585	5%	13%	4%	12%
		$\Delta R_p/R_p > 20\%$	$\Delta R_p/R_p < 20\%$	$\Delta R_p/R_p > 20\%$	$\Delta R_p/R_p < 20\%$
2021-2050	ssp126	3%	0%	3%	0%
	ssp245	6%	0%	6%	0%
	ssp585	3%	0%	2%	0%
2051-2100	ssp126	14%	0%	14%	0%
	ssp245	20%	0%	20%	0%
	ssp585	3%	6%	2%	5%

Rise and fall of vegetation primary production resilience to climate variability anticipated by a large ensemble of Earth System Models' simulations.

SUPPLEMENTARY MATERIAL

non-peer reviewed preprint submitted to EarthArXiv

Matteo Zampieri, Bruna Grizzetti, Andrea Toreti, Pierluca De Palma and Alessio Collalti

matteo.zampieri@ec.europa.eu

APPENDIX A:

Definition and properties of the annual production resilience indicator (R_p)

Assumptions

This theory focusses on production, which is a main ecosystem function. Other functions and features such as the internal structure and the relationships with the environment are not explicitly accounted for by the annual production resilience indicator.

The ecological and engineering definitions of resilience require the identification and the measurement of the system perturbations. Assuming that the larger perturbations are rarer compared to the smaller ones and that the larger perturbations result in larger production losses than the smaller ones, it is possible to quantify the amplitude of different types of perturbations and their combinations by a unique unit of measure that is the return period of the production losses (T^*). For annual production systems, T^* is the average number of years (or equivalently the inverse frequency) between events producing production losses of a certain amount.

Ecological resilience of homogeneous production systems ¹

This section describes the consistency between the annual production resilience indicator and the ecological definition of resilience. Following the Holling's definition of ecological resilience, we can define the annual production resilience as:

$$(1) R_{ecol} = T^*_{Max},$$

where T^*_{Max} is the largest pressure that the system can absorb before losing its production, measured by the return period of such events.

Using this definition, it is possible to demonstrate that production resilience can be estimated by the annual production resilience indicator:

$$(2) R_p = \mu^2 / \sigma^2,$$

where μ is the mean and σ the standard deviation of the production time-series.

The equivalence between equation 1 and 2 can be demonstrated for production systems that are homogeneous in space and time, meaning that the perturbations and the system response are spatially constant and that their statistical properties are stationary in time.

In the case the system production is binomially distributed, i.e., the annual production values are either the optimal production P in the years where $T^* < T^*_{Max}$ or zero in the years $T^* > T^*_{Max}$, the mean and the variance of the production are:

$$(3) \mu = P (1 - f), \text{ and}$$

$$(4) \sigma^2 = P^2 (1 - f) f,$$

where f is $1/T^*_{Max}$, the frequency of the years with zero production, which is assumed to be much smaller than the frequency of years with optimal production (adapted system). By combining equation 2 with 3 and 4 one obtains:

$$(5) R_p = (1 - f) / f \approx 1 / f = R_{ecol} \quad \text{Q.E.D.}$$

A more general relationship between the annual production resilience indicator (R_p) and the ecological resilience can be obtained with a modelling approach allowing the system to lose some of the production also for more common perturbations ($T^* < T^*_{Max}$), leading to the relationship:

$$(6) R_p = \alpha \cdot R_{ecol}, 0 < \alpha < 1$$

where α decreases the more the system is sensitive to common perturbations and the more the system bears the memory of the losses of the previous year, compromising the current year production.

Engineering resilience versus ecological resilience ²

This section describes the consistency between the ecological and engineering definitions of resilience for a special case. The engineering definition of resilience refers to the timing that the system takes to return to the equilibrium state after a disturbance and to recover its functional capacity.

In case of a linear production system, where the production is cumulated constantly in time and the return timing is proportional to the amplitude of the perturbation, it is possible to demonstrate the equivalence between the ecological and the engineering definitions of resilience.

Let Δp be the departure from the potential production (P) recorded at the end of the production cycle as a consequence of the perturbation that occurred during the production period. Let dt be the restoring time. No production takes place during this time.

Assuming a linear dependency between the production loss and that rareness of the event, the loss of production can be written as

$$(7) \Delta p' = dp'/dT^* \cdot T^*,$$

where dp'/dT^* is the derivative of the normalized production anomaly with respect to the amplitude of the perturbation. Using the chain rule of the derivative:

$$(8) \Delta p' = dp'/dt' \cdot dt'/dT^* \cdot T^*.$$

The first factor of equation 8 (dp'/dt') represents the derivative of the normalized production loss with respect to the normalized recovering time, which, under the linearity assumption, is equal to one because if the restoring time takes the entire production season ($dt'=1$), all the production is lost ($dp'=1$). So, this term can be eliminated by the equation, leading to:

$$(9) \Delta p' = dt'/dT^* \cdot T^*.$$

The factor dt'/dT^* in equations 8 and 9 is the derivative of the normalized recovering time with respect to the amplitude of the perturbation, measured by its return period. Thus, it represents the dependency of the production system recovering time from the amplitude of the perturbation. This term is clearly linkable to the engineering definition of resilience (R_{engin}):

$$(10) R_{engin} = 1 / (dt'/dT^*).$$

In fact, according to equation 10, when considering systems that are subject to the same external forcing, the more resilient system will be the one that returns more quickly to the normal functioning. If R_{engin} is infinite, the recovering is instantaneous ($dt'=0$) and there is no loss of production.

Using equations 9 and 10 and rearranging terms, R_{engin} can be written as the ratio between the return period of the external forcing and the normalized production anomaly:

$$(11) R_{engin} = T^* / \Delta\rho'$$

Evaluating equation (10) for $T^* = T^*_{MAX}$ and $\Delta\rho' = 1$, one obtains:

$$(12) R_{engin} = T^*_{MAX} = R_{ecol}$$

which is the ecological definition of resilience Q.E.D..

Therefore, the annual production resilience indicator is in principle consistent with the engineering definition of resilience as well. However, the assumption of linearity of the production system is seldom verified in real production system. This assumption is invoked in this section only and does not affect the rest of the theory.

Non-stationary production systems ³

The annual production resilience indicator (R_p) is not well-defined for time-series where the production mean is changing in time, because the mean and the standard deviation are ill-defined in the first place. In this case, it is possible to normalize the production time-series by a moving average, or by a non-linear fitting algorithm before computing R_p .

In case the time-series is stationary, this procedure does not change the annual production resilience value. In case it is not, it allows to remove the trend accounting for the fluctuations proportionally, so that the departures from the mean in the periods with higher production are not penalized with respect to those with lower production.

Heterogeneous production systems – Effects of diversity on production resilience ¹

Real production systems are often characterized by some degree of spatial variability of the perturbations and of the production response by different species (γ -diversity). The production time-series recorded from spatially heterogeneous systems can be treated as the linear superposition of individual homogeneous production systems. In this case, the effect of diversity on the value annual production resilience indicator computed from the total production time-series can be easily understood by induction. Let us consider a production system composed of two independent production sources. The mean and the variance of this production system are:

$$(13) \mu_{TOT} = \mu_1 + \mu_2, \text{ and}$$

$$(14) \sigma^2_{TOT} = \sigma^2_1 + \sigma^2_2 + 2 \cdot Cov_{1,2}$$

where Cov is the covariance between the two production time-series.

If the time-series have same mean and standard deviation and they are not correlated with each other, the annual production resilience indicator of the sum is exactly the double of that of the individual time-series. In case they are totally correlated, the total production resilience equals that of the individual time-series. Whereas, if they are totally anticorrelated, the individual fluctuations are exactly balanced between each other, the variance is zero and the total production resilience indicator becomes infinite.

In case there are n uncorrelated time-series with same mean and variance, the annual production resilience of their sum is exactly n -times the value of the individual time series and the probability of total production loss gets extremely low. This is the reason why total production loss is very rarely observed in production time-series recorded over large areas. In case the total production is unevenly distributed among the different time series, the time-series with larger production contributed proportionally more than the others. In case the time-series are partially

correlated/anticorrelated, they contribute less/more to the increase of total production resilience. In case there is a component of the system that does not contribute to resilience such as non-vegetated area within the region under evaluation, this is not contributing to the total production resilience and does not change the value of the annual production resilience indicator ⁴.

Accuracy of the annual production resilience indicator ¹

The accuracy of R_p can be evaluated by Monte-Carlo experiments. For normally distributed time-series, which often characterize real production systems, the sampling error of the annual production resilience indicator is roughly the 30%, if computed on time-series of about 30 numbers. Other reference values can be inferred from a look up table.

References

1. Zampieri, M. *et al.* Estimating resilience of crop production systems: From theory to practice. *Sci. Total Environ.* **735**, 139378 (2020).
2. Zampieri, M. Reconciling the ecological and engineering definitions of resilience. *Ecosphere* (2021) doi:<https://doi.org/10.1002/ecs2.3375>.
3. Zampieri, M. *et al.* Climate resilience of the top ten wheat producers in the Mediterranean and the Middle East. *Reg. Environ. Chang.* **20**, 41 (2020).
4. Zampieri, M. *et al.* Annual Green Water Resources and Vegetation Resilience Indicators: Definitions, Mutual Relationships, and Future Climate Projections. *Remote Sens.* **11**, 2708 (2019).

APPENDIX B

Supplementary Figures and Tables

Figure S1 S2 S3 and the second column of Table S2 can be qualitatively compared to Zampieri et al.⁴, where vegetation production for a similar period (1982-2015 instead of 1985-2014) was estimated using the Normalized Differential Vegetation Index (NDVI) measured by remote sensing as proxy of the observed gross primary production. It is worth noting that in Zampieri et al. the annual NDVI mean was computed from January to December, not considering the shift in growing seasons as in the present paper.

Fig S1: ensemble median GPP average (Kg/year)

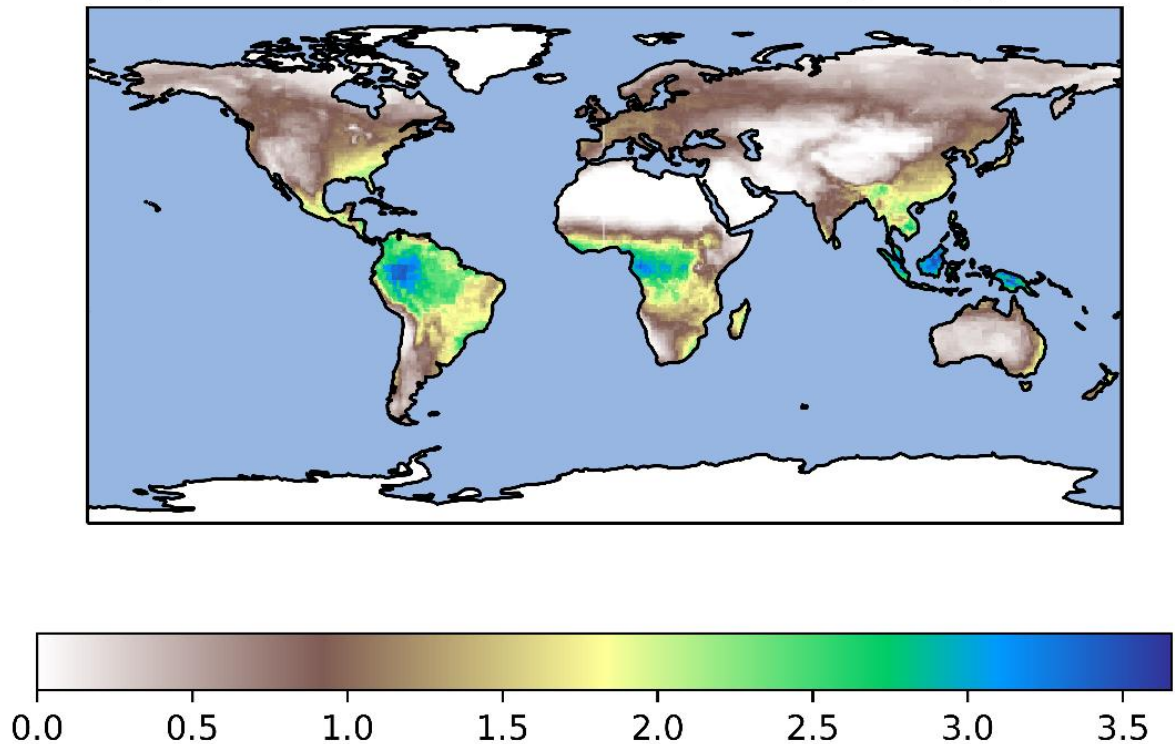


Fig S2: ensemble GPP variability (Kg/year)

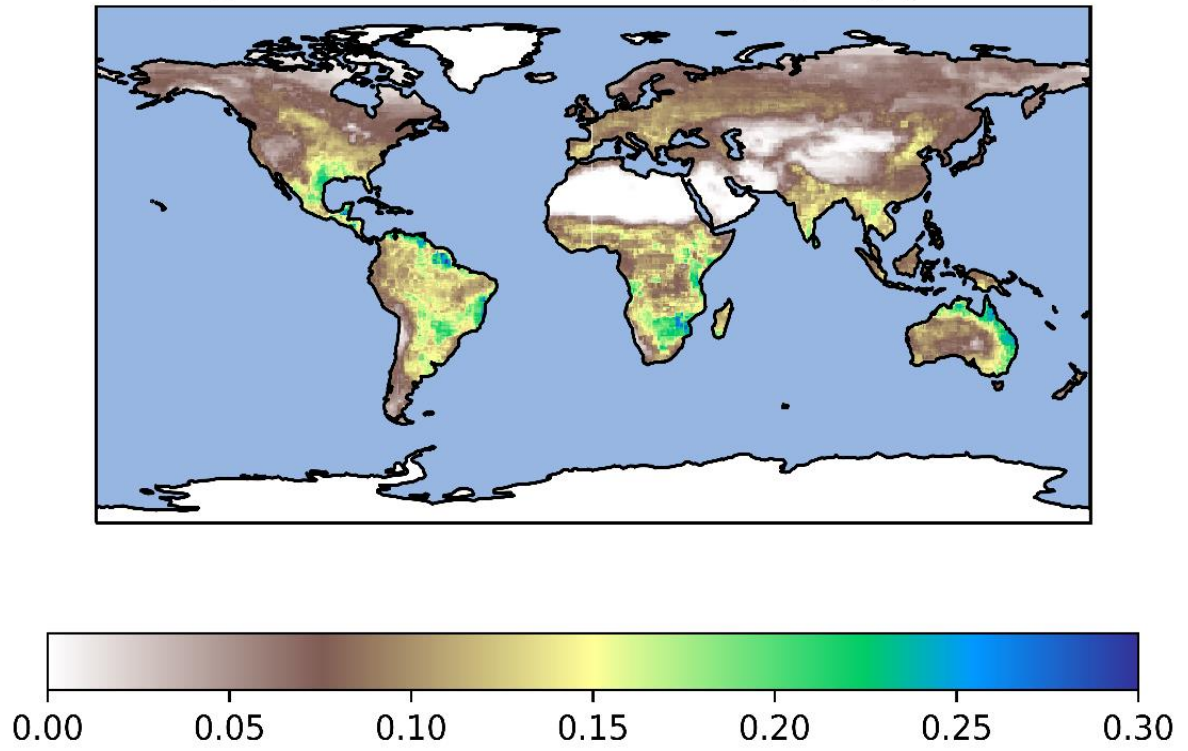
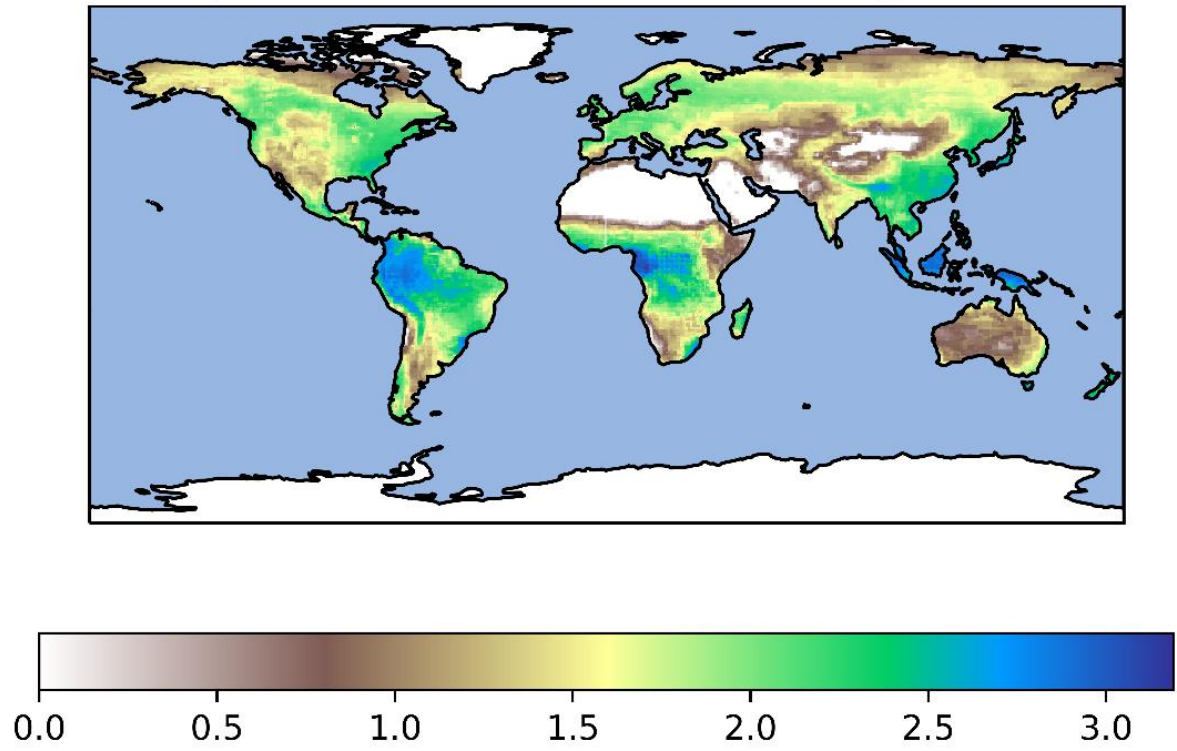


Fig S3: ensemble GPP resilience $\log_{10}(R_v)$



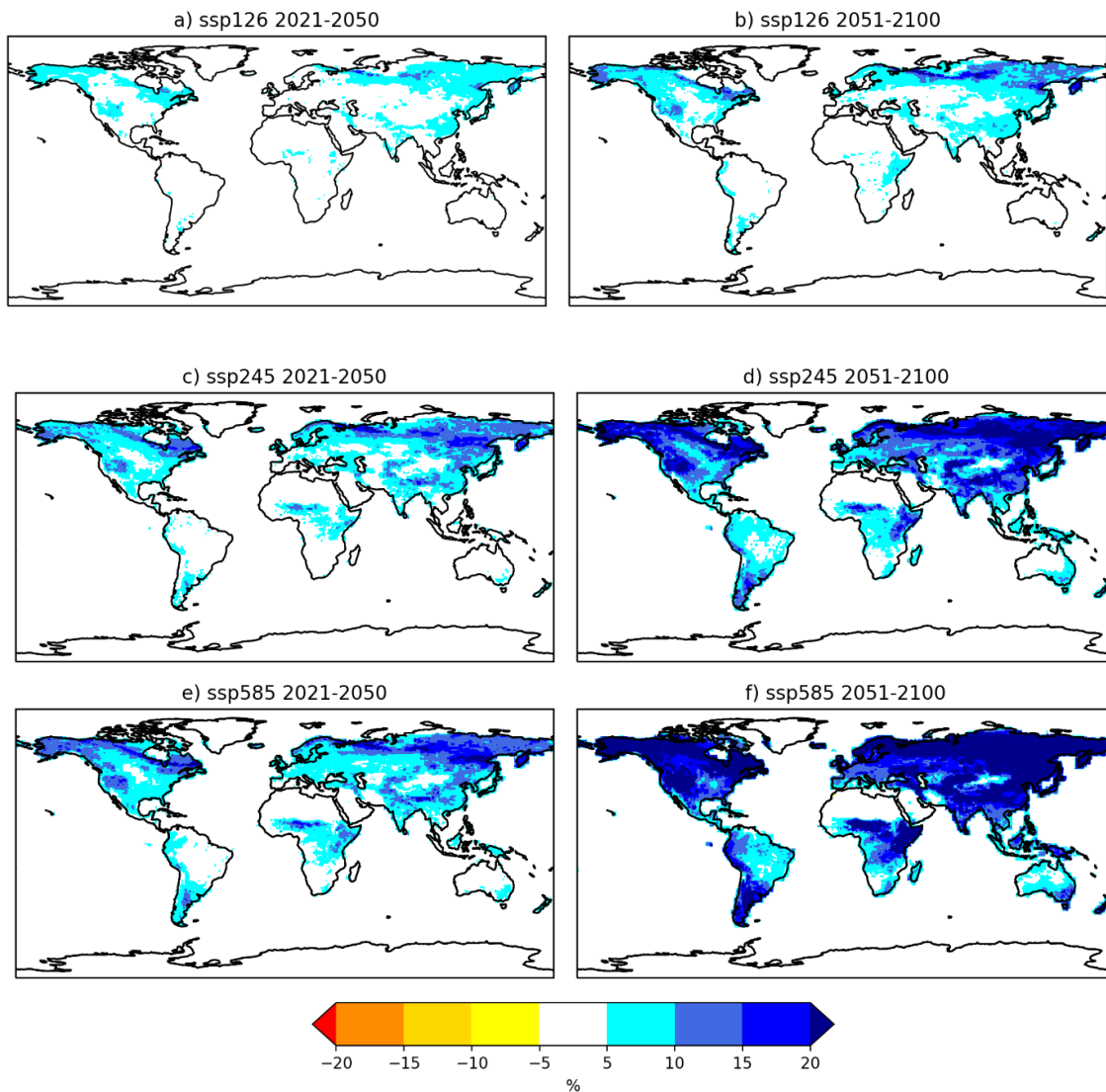


Figure S4. Global changes of annual gross primary production computed from an ensemble of 16 Earth System Models (ESMs) simulations under ssp126 (panels a and b), ssp245 (panels c and d), and ssp585 (panels e and f) CMIP6 scenarios in the periods 2021-2050 (panels a, c, and e) and 2051-2100 (panels b, d, and f) compared to the period 1985-2014.

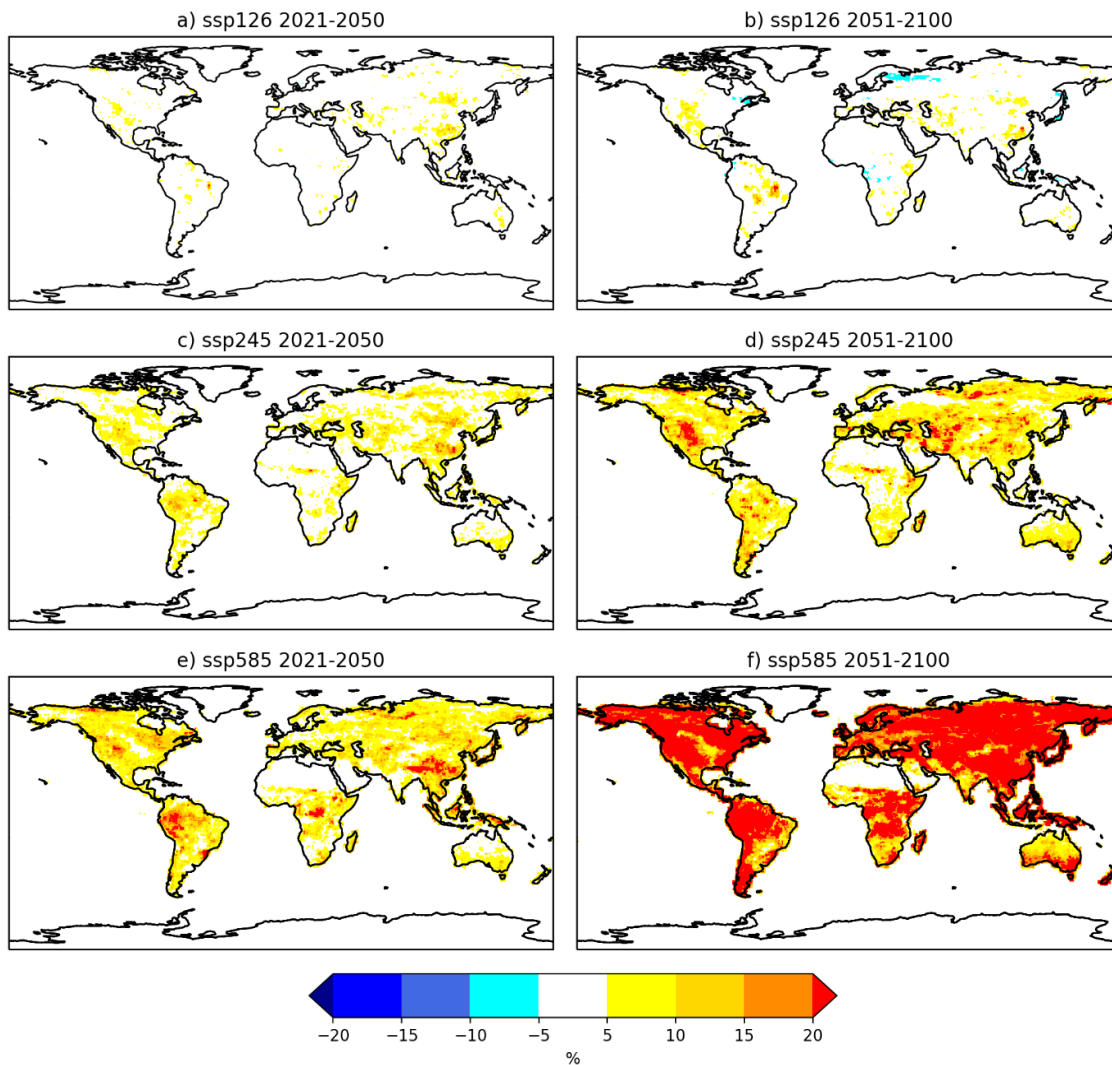


Figure S5. Global changes of annual gross primary production standard deviation computed from an ensemble of 16 Earth System Models (ESMs) simulations under ssp126 (panels a and b), ssp245 (panels c and d), and ssp585 (panels e and f) CMIP6 scenarios in the periods 2021-2050 (panels a, c, and e) and 2051-2100 (panels b, d, and f) compared to the period 1985-2014.

Table S1: Koppen Climates classification (koeppen-geiger.vu-wien.ac.at)

Main Climates	Precipitation	Temperature	
A: equatorial	W: desert	h: hot arid	F: polar frost
B: arid	S: steppe	k: cold arid	T: polar tundra
C: warm temperature	f: fully humid	a: hot summer	
D: snow	s: summer dry	b: warm summer	
E: polar	w: winter dry	c: cool summer	
	m: monsoonal	d: extremely continental	

Table S2: Fraction of biome areas where the relative resilience indicator ($\Delta R_p/R_p$) exceeds the 15% in the simulation ensemble median in the Green Road scenario (ssp126) in 2021-2051 (g) and in 2051-2100 (G), in the Middle of the Road scenario (ssp245) in 2021-2051 (m) and in 2051-2100 (M) and in the Fossil Fuel scenario (ssp585) in 2021-2051 (f) and in 2051-2100 (F). Plus and minus signs refer to positive and negative changes, i.e. $\Delta R_p/R_p > 15\%$ and $\Delta R_p/R_p < -15\%$, respectively. The biome areas are considered according to the Koppen-climates classifications (see Table 1). The spatial distribution of Koppen-climates classification has been downloaded from koeppen-geiger.vu-wien.ac.at

Clim	Mean R _p	g+	G+	m+	M+	f+	F+	g-	G-	m-	M-	f-	F-
Af	491±235	0	0	0	9	2	0	0	1	22	0	1	65
Am	290±206	0	0	0	6	2	0	0	5	14	0	3	48
As	132±255	1	2	0	8	5	4	0	0	0	0	0	10
Aw	154±161	0	3	1	4	4	3	0	1	3	2	2	26
BWk	5±9	0	1	0	0	11	4	0	0	0	0	0	0
BWh	3±12	0	0	0	0	1	3	0	0	0	0	0	0
BSk	21±26	0	0	0	1	3	0	0	0	0	0	0	5
BSh	26±35	0	5	3	0	6	9	0	0	0	0	0	4
Cfa	156±134	0	0	0	9	4	2	0	1	5	0	0	16
Cfb	138±116	1	6	1	11	10	1	0	0	2	0	1	18
Cfc	120±78	1	11	2	12	11	0	0	0	2	0	0	24
Csa	29±22	1	2	2	0	2	3	0	0	0	0	3	16
Csb	75±64	0	0	0	1	1	0	0	0	0	0	0	16
Csc	62±28	0	0	0	0	9	0	0	0	0	0	0	45
Cwa	150±102	0	2	0	2	1	1	0	1	6	0	1	34
Cwb	180±113	0	2	1	10	5	3	0	3	13	0	2	54
Cwc	160±87	0	0	0	10	0	0	0	0	0	0	0	80
Dfa	50±45	0	1	0	1	4	0	0	0	0	0	0	2
Dfb	81±52	3	6	0	17	22	0	0	0	0	0	0	14
Dfc	51±35	25	40	16	57	77	5	0	0	0	0	0	6
Dfd	22±13	19	51	40	71	83	30	0	0	0	0	0	0
Dsa	20±11	0	1	0	0	1	0	0	0	0	0	0	1
Dsb	42±31	0	0	1	1	2	0	0	0	0	0	1	10
Dsc	36±24	36	29	10	68	79	0	0	0	0	0	0	2
Dwa	107±69	0	0	0	4	7	1	0	0	0	0	0	4
Dwb	115±73	2	1	0	28	21	0	0	0	1	0	0	12
Dwc	57±32	22	17	1	52	53	0	0	0	0	0	0	12
Dwd	32±8	8	51	10	89	98	0	0	0	0	0	0	0
ET	14±30	8	21	15	26	58	18	0	0	0	0	0	2
EF	0±0	0	0	0	0	0	0	0	0	0	0	0	0

Table S3. Fraction of country areas where the relative resilience indicator ($\Delta R_p/R_p$) exceeds the 15% in the simulation ensemble median in the Green Road scenario (ssp126) in 2021-2051 (g) and in 2051-2100 (G), in the Middle of the Road scenario (ssp245) in 2021-2051 (m) and in 2051-2100 (M) and in the Fossil Fuel scenario (ssp585) in 2021-2051 (f) and in 2051-2100 (F). Plus and minus signs refer to positive and negative changes, i.e. $\Delta R_p/R_p > 15\%$ and $\Delta R_p/R_p < -15\%$, respectively.

ISO3	g+	G+	m+	M+	f+	F+	g-	G-	m-	M-	f-	F-	Country Name
ARE	0	0	0	0	0	0	0	0	0	0	0	0	United Arab Emirates
AFG	0	0	0	2	1	0	0	0	0	0	0	0	Afghanistan
ALB	0	0	0	0	0	0	0	0	0	0	0	0	Albania
ARM	0	0	0	0	0	0	0	0	0	0	0	8	Armenia
AGO	0	1	0	4	0	1	0	0	0	0	7	45	Angola
ATA	0	0	0	0	0	0	0	0	0	0	0	0	Antarctica
ARG	0	2	0	2	0	5	0	0	0	0	2	9	Argentina
AUT	3	21	33	36	3	0	0	0	0	0	0	16	Austria
AUS	0	0	0	0	0	0	0	0	0	1	0	4	Australia
AZE	0	0	0	0	0	0	0	0	0	0	0	1	Azerbaijan
BIH	0	0	0	0	0	0	0	0	0	0	0	0	Bosnia and Herzegovina
BGD	0	0	26	19	0	0	0	0	0	0	0	0	Bangladesh
BEL	0	0	0	0	0	0	0	0	0	0	0	12	Belgium
BFA	1	0	21	8	7	36	0	0	0	0	0	0	Burkina Faso
BGR	0	0	0	0	0	0	0	0	0	0	0	0	Bulgaria
BDI	0	0	0	0	0	0	0	0	0	0	0	0	Burundi
BEN	0	3	8	8	3	18	0	0	0	0	0	0	Benin
BRN	0	0	0	0	0	0	0	0	0	0	0	100	Brunei Darussalam
BOL	0	0	0	0	0	0	0	13	13	9	11	67	Bolivia
BRA	0	0	0	0	0	0	1	4	4	6	20	57	Brazil
BHS	0	0	0	0	0	0	0	0	0	0	0	0	Bahamas
BTN	0	54	0	8	0	0	0	0	0	0	15	85	Bhutan
BWA	0	0	0	0	0	0	0	0	0	0	0	0	Botswana
BLR	0	6	0	9	0	0	0	0	0	0	0	0	Belarus
BLZ	0	0	0	0	0	0	0	0	0	0	0	0	Belize
CAN	12	38	25	52	5	4	0	0	0	0	0	15	Canada
COD	1	23	0	9	0	0	0	0	0	0	20	26	Congo DR
CAF	2	12	5	19	1	1	0	0	0	0	0	8	Central African Republic
COG	2	31	0	4	0	0	0	0	0	0	4	71	Congo
CHE	0	66	66	78	0	0	0	0	0	0	0	11	Switzerland
CIV	0	0	5	1	0	1	0	0	0	0	3	2	Côte d'Ivoire
COK	0	0	0	0	0	0	0	0	0	0	0	0	Cook Islands
CHL	0	3	0	2	0	0	0	0	0	1	0	29	Chile
CMR	1	18	1	6	0	3	0	0	0	0	20	44	Cameroon
CHN	1	11	4	21	1	3	0	0	0	0	4	17	China
COL	1	19	0	2	0	0	0	0	0	0	10	52	Colombia
CRI	0	7	0	0	0	0	0	0	0	0	0	53	Costa Rica
CUB	0	0	0	0	0	0	0	0	0	0	0	0	Cuba
CPV	0	0	0	0	0	0	0	0	0	0	0	0	Cabo Verde
CYP	0	0	0	0	0	0	0	0	0	0	0	100	Cyprus
CZE	0	13	3	40	3	0	0	0	0	0	0	0	Czech Republic
DEU	0	20	8	26	4	0	0	0	0	0	0	0	Germany
DJI	0	0	0	0	0	43	0	0	0	0	0	0	Djibouti
DNK	3	0	58	51	24	0	0	0	0	0	0	0	Denmark

DOM	0	0	0	0	0	0	0	0	0	0	0	6	Dominican Republic
DZA	0	0	0	0	0	0	0	0	0	0	0	1	Algeria
ECU	0	33	0	2	0	0	0	0	0	0	2	58	Ecuador
EST	0	7	0	37	0	0	0	0	0	0	0	4	Estonia
EGY	1	2	2	1	1	1	0	0	0	0	0	0	Egypt
ERI	0	0	0	0	0	5	0	0	0	0	0	0	Eritrea
ESP	0	0	0	0	0	0	0	0	0	3	0	17	Spain
ETH	0	1	7	9	3	22	0	0	0	0	0	0	Ethiopia
FIN	52	87	53	99	11	0	0	0	0	0	0	0	Finland
FJI	0	0	0	0	0	0	0	0	0	0	0	0	Fiji
FLK	0	0	0	0	0	0	0	0	0	0	0	50	Falkland Islands
FRO	0	0	0	0	0	0	0	0	0	0	0	0	Faroe Islands
FRA	0	3	1	9	0	0	0	0	0	2	0	12	France
GAB	5	60	0	0	0	0	0	0	0	0	2	87	Gabon
GBR	12	38	34	30	0	0	0	0	0	0	0	4	United Kingdom
GEO	0	0	0	0	0	0	0	0	0	0	0	7	Georgia
GUF	0	0	0	0	0	0	0	0	0	0	0	15	French Guiana
GHA	0	0	11	8	0	0	0	0	0	0	0	0	Ghana
GRL	0	0	1	2	1	1	0	0	0	0	0	0	Greenland
GMB	0	0	0	0	0	0	0	0	0	0	0	0	Gambia
GIN	0	1	5	1	0	0	0	0	0	0	0	12	Guinea
GLP	0	0	0	0	0	0	0	0	0	0	0	0	Guadeloupe
GNQ	0	89	0	0	0	0	0	0	0	0	0	78	Equatorial Guinea
GRC	0	0	0	0	0	0	0	0	0	0	0	10	Greece
SGS	0	0	0	0	0	0	0	0	0	0	0	0	South Georgia and South Sandwich Islands
GTM	0	0	0	0	0	0	0	0	0	0	0	39	Guatemala
GNB	0	0	0	0	0	0	0	0	0	0	0	0	Guinea-Bissau
GUY	0	0	0	0	0	0	0	0	0	5	5	76	Guyana
HND	0	0	0	0	0	0	0	0	0	3	0	67	Honduras
HRV	0	0	0	0	0	0	0	0	0	0	0	0	Croatia
HTI	0	0	0	0	0	0	0	0	0	0	0	8	Haiti
HUN	0	0	0	0	0	0	0	0	0	0	0	0	Hungary
IDN	0	16	1	4	0	0	0	0	0	1	11	58	Indonesia
IRL	0	13	31	18	0	0	0	0	0	0	0	5	Ireland
ISR	0	0	0	0	0	0	0	0	0	0	0	0	Israel
IND	3	3	8	16	2	7	0	0	0	0	1	6	India
IRQ	0	0	0	0	0	0	0	0	0	0	2	1	Iraq
IRN	0	0	0	0	0	0	0	0	0	0	0	0	Iran
ISL	3	4	58	87	46	7	0	0	0	0	0	0	Iceland
ITA	0	1	0	1	0	0	0	0	0	0	0	3	Italy
JAM	0	0	0	0	0	0	0	0	0	0	0	0	Jamaica

JOR	0	0	0	0	0	0	0	0	0	0	0	0	Jordan
JPN	0	90	1	4	0	0	0	0	0	0	8	75	Japan
KEN	0	0	0	13	1	29	0	0	0	0	0	0	Kenya
KGZ	0	0	0	19	0	0	0	0	0	0	0	8	Kyrgyzstan
KHM	0	0	0	0	0	0	0	0	0	0	13	50	Cambodia
KIR	0	0	0	0	0	0	0	0	0	0	0	0	Kiribati
COM	0	0	0	0	0	0	0	0	0	0	0	0	Comoros
PRK	0	15	0	0	0	0	0	0	0	0	8	58	North Korea
KOR	0	53	0	0	0	0	0	0	0	0	0	64	South Korea
KWT	0	0	0	0	0	0	0	0	0	0	0	0	Kuwait
KAZ	0	0	1	4	0	0	0	0	0	0	0	0	Kazakhstan
LAO	0	0	0	0	0	0	0	0	0	0	19	59	Laos
LBN	0	0	0	0	0	0	0	0	0	0	0	75	Lebanon
LKA	0	9	9	59	0	0	0	0	0	0	0	0	Sri Lanka
LBR	0	6	0	0	0	0	0	0	0	0	10	10	Liberia
LSO	0	0	0	0	0	0	0	0	0	0	0	58	Lesotho
LTU	31	36	3	38	0	0	0	0	0	0	0	0	Lithuania
LUX	0	100	0	100	0	0	0	0	0	0	0	0	Luxembourg
LVA	0	6	0	66	0	0	0	0	0	0	0	0	Latvia
LBY	0	0	0	0	0	0	0	0	0	0	0	0	Libya
MAR	0	0	0	0	0	0	0	0	0	5	0	17	Morocco
MDA	0	0	0	0	0	0	0	0	0	0	0	0	Moldova
MNE	0	0	0	0	0	0	0	0	0	0	0	0	Montenegro
MDG	2	0	0	0	0	0	0	0	0	12	14	55	Madagascar
MKD	0	0	0	0	0	0	0	0	0	0	0	0	The Former Yugoslav Republic of Macedonia
MLI	0	0	6	4	1	2	0	0	0	0	0	1	Mali
MMR	0	2	0	0	0	0	0	0	0	1	7	38	Myanmar
MNG	0	2	0	5	0	1	0	0	0	0	0	2	Mongolia
MRT	0	0	0	2	0	0	0	0	0	0	0	0	Mauritania
MUS	0	0	0	0	0	0	0	0	0	0	0	0	Mauritius
MWI	0	0	0	0	0	0	0	0	0	0	0	39	Malawi
MEX	0	0	0	0	0	0	0	0	0	0	1	14	Mexico
MYS	0	20	1	1	0	0	0	0	0	0	7	77	Malaysia
MOZ	0	0	0	0	0	0	0	0	0	0	1	19	Mozambique
NAM	0	0	0	0	0	0	0	0	0	0	0	1	Namibia
NCL	0	0	0	0	0	0	0	0	0	0	0	0	New Caledonia
NER	0	0	11	8	13	22	0	0	0	0	0	0	Niger
NGA	2	1	24	11	16	34	0	0	0	0	0	0	Nigeria
NIC	0	0	0	0	0	0	0	0	0	4	0	59	Nicaragua
NLD	0	0	0	0	0	0	0	0	0	0	0	0	Netherlands
NOR	14	38	70	73	10	0	0	0	0	0	0	14	Norway

NPL	0	19	2	4	0	0	0	0	0	0	0	19	Nepal
NZL	2	21	0	7	0	0	0	0	0	0	0	32	New Zealand
OMN	0	0	0	0	0	0	0	0	0	0	0	0	Oman
PAN	0	4	0	4	0	0	0	0	0	0	0	25	Panama
PER	0	9	0	2	0	0	0	0	0	0	33	76	Peru
PYF	0	0	0	0	0	0	0	0	0	0	0	0	French Polynesia
PNG	0	8	0	2	0	0	0	0	0	0	19	62	Papua New Guinea
PHL	0	0	0	0	0	0	0	0	0	0	15	59	Philippines
PAK	0	1	0	5	2	3	0	0	0	0	0	0	Pakistan
POL	0	2	0	0	0	0	0	0	0	0	0	0	Poland
PRI	0	0	0	0	0	0	0	0	0	0	0	0	Puerto Rico
PSE	0	0	0	0	0	0	0	0	0	0	0	0	Palestinian Territory
PRT	0	0	0	0	0	0	0	0	0	2	0	31	Portugal
PRY	0	1	0	0	0	2	0	1	1	6	4	1	Paraguay
QAT	0	0	0	0	0	0	0	0	0	0	0	0	Qatar
REU	0	0	0	0	0	0	0	0	0	0	0	0	RÅ©union
ROU	0	0	0	0	0	0	0	0	0	1	0	1	Romania
SRB	0	0	0	0	0	0	0	0	0	0	0	0	Serbia
RUS	22	51	31	68	16	7	0	0	0	0	0	3	Russian Federation
RWA	0	40	0	0	0	0	0	0	0	0	0	0	Rwanda
SAU	0	0	0	0	0	0	0	0	0	0	0	0	Saudi Arabia
SLB	0	0	0	0	0	0	0	0	0	0	0	20	Solomon Islands
SDN	0	0	4	3	1	7	0	0	0	0	0	0	Sudan
SWE	19	60	55	83	11	0	0	0	0	0	0	4	Sweden
SVN	0	0	0	0	0	0	0	0	0	0	0	0	Slovenia
SJM	0	0	0	0	0	1	0	0	0	0	0	0	Jan Mayen
SVK	0	0	0	0	0	0	0	0	0	0	0	0	Slovakia
SLE	12	24	8	0	0	0	0	0	0	0	0	12	Sierra Leone
SEN	0	0	0	0	0	0	0	0	0	0	0	10	Senegal
SOM	0	0	0	31	0	66	0	0	0	0	0	0	Somalia
SUR	0	0	0	0	0	0	0	0	0	0	0	43	Suriname
SSD	1	0	5	10	2	0	0	0	0	0	0	1	South Sudan
STP	0	0	0	0	0	0	0	0	0	0	0	0	Sao Tome and Principe
SLV	0	0	0	0	0	0	0	0	0	0	0	100	El Salvador
SYR	0	0	0	0	0	0	0	0	0	1	0	3	Syria
SWZ	0	0	0	0	0	0	0	0	0	0	0	0	Swaziland
TCD	2	0	14	10	8	12	0	0	0	0	0	0	Chad
ATF	0	0	0	0	0	0	0	0	0	0	0	0	French Southern Territories
TGO	0	6	22	22	6	0	0	0	0	0	0	0	Togo
THA	0	0	1	1	0	0	0	0	0	0	2	3	Thailand
TJK	0	0	0	2	0	0	0	0	0	0	0	2	Tajikistan

TLS	0	0	0	0	0	0	0	0	0	0	0	0	Timor-Leste
TKM	0	0	0	0	0	0	0	0	0	0	0	0	Turkmenistan
TUN	0	0	0	0	0	0	0	0	0	0	0	12	Tunisia
TUR	0	0	0	1	0	0	0	0	0	2	0	15	Turkey
TTO	0	0	0	0	0	0	0	0	0	0	0	100	Trinidad and Tobago
TZA	0	1	0	13	2	25	0	0	0	0	5	2	Tanzania
UKR	0	0	0	0	0	0	0	0	0	0	0	1	Ukraine
UGA	0	2	0	20	2	22	0	0	0	0	0	0	Uganda
USA	8	17	9	21	5	1	0	0	0	0	0	11	United States
URY	0	0	0	1	0	0	0	0	0	0	0	0	Uruguay
UZB	0	0	0	0	0	0	0	0	0	0	0	1	Uzbekistan
VCT	0	0	0	0	0	0	0	0	0	0	0	0	Saint Vincent and the Grenadine
VEN	0	0	0	0	0	0	0	0	0	0	12	80	Venezuela
VIR	0	0	0	0	0	0	0	0	0	0	0	0	US Virgin Islands
VNM	0	0	0	0	0	0	0	0	0	0	11	46	Vietnam
VUT	0	0	0	0	0	0	0	0	0	0	0	0	Vanuatu
WS M	0	0	0	0	0	0	0	0	0	0	0	0	Samoa
YEM	0	0	0	0	0	0	0	0	0	0	0	0	Yemen
ZAF	0	0	0	0	0	0	0	0	0	1	1	12	South Africa
ZMB	0	0	0	0	0	0	0	0	0	2	4	66	Zambia
ZWE	0	0	0	0	1	0	0	0	0	0	0	1	Zimbabwe